A Comparison of Vector-Sensing and Scalar-Sensing Linear Arrays

Benjamin A. Cray
Submarine Sonar Department

Albert H. Nuttall
Surface Undersea Warfare Directorate

Naval Undersea Warfare Center Division
Newport, Rhode Island

19970328 056

PREFACE

Reviewed and Approved: 27 January 1997

R. J. Martin
Head, Submarine Sonar Department

REPORT DOCUMENTATION PAGE

Public reporting burden for this collection of information is estimated to average 1 hour per response, including the time for reviewing instructions, searching existing data sources, gathering and maintaining the data needed, and completing and reviewing the collection of information. Send comments regarding this burden estimate or any other aspect of this collection of information, including suggestions for reducing this burden, to Washington Headquarters Services, Directorate for Information Operations and Reports, 1215 Jefferson Davis Highway, Suite 1204, Arlington, VA 22202-4302, and to the Office of Management and Budget, Paperwork Reduction Project (0704-0188), Washington, DC 20503.

1. AGENCY USE ONLY (Leave Blank)	2. REPORT DATE	3. REPORT TYPE AND DATES COVERED
	27 January 1997	Final

4. TITLE AND SUBTITLE

A Comparison of Vector-Sensing and Scalar-Sensing Linear Arrays

5. FUNDING NUMBERS

PR H60030
PR B10007

6. AUTHOR(S)

Benjamin A. Cray and Albert H. Nuttall

7. PERFORMING ORGANIZATION NAME(S) AND ADDRESS(ES)

Naval Undersea Warfare Center Division
1176 Howell Street
Newport, Rhode Island 02841

8. PERFORMING ORGANIZATION REPORT NUMBER

TR 10,632

9. SPONSORING/MONITORING AGENCY NAME(S) AND ADDRESS(ES)

Office of Naval Research (Code 321SS)
800 North Quincy Street
Arlington, Virginia 22217

10. SPONSORING/MONITORING AGENCY REPORT NUMBER

11. SUPPLEMENTARY NOTES

12a. DISTRIBUTION/AVAILABILITY STATEMENT

Approved for public release; distribution is unlimited.

12b. DISTRIBUTION CODE

Some of the features which are unique to beamforming a linear array of vector sensors, not present with scalar-sensing elements (such as conventional pressure sensors), are described in this report. Vector sensors measure acoustic particle motion, for example acoustic particle velocity, in a given direction and these vectors have complex-valued components which are proportional to the amplitude and phase of a propagating acoustic field. Three types of vector sensors are considered; a uniaxial vector sensor which measures acoustic particle velocity along a single axis, a biaxial vector sensor measuring velocity in two orthogonal directions, and a triaxial sensor which measures all three orthogonal components of the velocity vector.

Comparisons are made between the performance (in terms of received element and array sensitivity, array directivity, and signal gain with array curvature) of arrays comprised of each type of vector sensor, to arrays comprised of pressure sensors only. The comparisons have also evaluated two boundary conditions, perfectly baffled sensors and sensors in the free field. It is shown that a *single* triaxial vector sensor may be steered, in both azimuth and elevation, to any planewave arrival direction. A single pressure sensor provides no directivity in the free field. A comparison of array directivity indicates (for optimal real-valued amplitude shading coefficients) that triaxial and biaxial vector sensors can provide 5 dB of directivity gain over that obtained from an identical array of pressure sensors. The gain varies with the direction the array is steered to. Similarly, multiaxis vector sensors improve a conformal array's signal gain for all array steerings. For a cylindrically-curved vertical array, vector sensors improved signal gain by a minimum of approximately 3 dB at 45 degree steerings, to a maximum gain of 4 dB at broadside.

It has also been shown that, unlike pressure-sensors, there exist no interelement array spacing at which vector components are all uncorrelated with themselves for a spherically isotropic field. Thus, even for half-wavelength spacing, element noise correlations must be accounted for in any signal detection procedure.

14. SUBJECT TERMS		15. NUMBER OF PAGES
Acoustic Vector Sensors	Submarine Sonar Systems	40
Scalar Pressure Sensors	Velocity Sensors	**16. PRICE CODE**

17. SECURITY CLASSIFICATION OF REPORT	18. SECURITY CLASSIFICATION OF THIS PAGE	19. SECURITY CLASSIFICATION OF ABSTRACT	20. LIMITATION OF ABSTRACT
Unclassified	Unclassified	Unclassified	SAR

TABLE OF CONTENTS

LIST OF ILLUSTRATIONS

LIST OF ILLUSTRATIONS (Cont'd)

A COMPARISON OF VECTOR-SENSING AND SCALAR-SENSING LINEAR ARRAYS

INTRODUCTION

Unlike scalar pressure sensors, acoustic vector sensors measure the amplitude and phase of acoustic particle motion in a given direction. These sensors, generally referred to as velocity sensors, measure a vector quantity, i.e., acoustic particle acceleration, velocity, or displacement. A single-axis, or uniaxis, acoustic vector sensor will be defined here as a sensor that measures one (cartesian) component of the acoustic field vector. Biaxial vector sensors, such as biaxial accelerometers, denote sensors that measure motion in two orthogonal directions, while triaxial vector sensors measure all three orthogonal components. These uniaxis and multiaxis vector sensors can then be configured into an array of elements, the elements of which may be delayed, weighted, and summed, as commonly done with standard pressure hydrophones. However, there are some unique features present in the beamforming of vector sensors that are not present with pressure sensors. This report will describe some of these unique features, i.e., the differences between arrays of scalar pressure sensors and arrays composed of acoustic vector sensors.

REVIEW OF PREVIOUS RESEARCH

A brief literary review indicates that a group of researchers[1-4] have recently documented some aspects of beamforming arrays of multiple-axis vector sensors. D'Spain[1] constructed and deployed a 16-element vertical line array that measured the three components of free-field acoustic particle velocity as well as acoustic pressure. The low frequency DIrectional low Frequency Analysis and Recording (DIFAR) array consisted of collocated pressure hydrophones with three orthogonally mounted geophones. The output from a geophone sensor is directly proportional to acoustic particle velocity. At-sea data collected from the array were beamformed conventionally (delayed and summed with uniform amplitude weighting) and adaptively, using a minimum variance Capon approach on all four quantities.

Nehorai[2] developed an analytical model to compare the direction-of-arrival (DOA) estimation performance of an array of sensors, which measures acoustic pressure and all three components of acoustic particle velocity, to that of an array which measures acoustic pressure only. The paper treated both single and multiple acoustic sources in an ideal free-field environment. Cramer-Rao lower bounds (CRLB) on DOA estimation for the single-source single-vector sensor as well as multiple-source multivector sensors were given. The CRLB provides a universal measure of achievable estimation accuracy and is commonly used by signal processors to compare the merits of different high-resolution DOA methods. Hawkes[3] extended the work of Nehorai by introducing a plane boundary at or near the vector-sensing array. As done previously in the paper by Nehorai, expressions for the CRLB were derived and analyzed

for various stand-off distances from ideal pressure-release and rigid boundaries. In reference 4, Kneipfer, using notation and formulations common to the sonar community, rederived some of the analytical model developed by Nehorai. The work reported here is a continuation of Kneipfer's preliminary efforts, examining in additional detail the merits of vector-sensing arrays.

MODEL OF ARRAY RESPONSE

This section will develop a model for the beamformed response of uniaxial, biaxial, and triaxial arrays of vector sensors which measure acoustic particle velocity in the free field and on an idealized boundary. The boundary is assumed to provide perfect baffling of half the free-field acoustic field and ideal pressure-release behavior for *each* orthogonal acoustic velocity component. The baffled and free-field vector array responses are compared to that of a similar array of scalar pressure sensors. The effects of a nonideal boundary, such as a submarine hull coating, may be incorporated in future investigations. It is important to stress that these comparisons have been made in order to assess the merits of an array of vector sensors to an array of scalar sensors based on *ideal* conditions. If the benefits of vector-sensing are significant, then subsequent investigations can incorporate realistic boundary behavior. Keltie[5] has investigated a realistic solid-layer model for typical submarine hull coatings, which models both the coating's tangential and normal signal-induced velocities. If warranted, his results may be incorporated into the model developed here.

Each multiaxis-vector sensor will be assumed to be collocated, measuring three orthogonal components of particle velocity at the same spatial location. Such a restriction may not be optimal for detection but is used here to simplify the formulation. Figure 1 illustrates the array geometry and coordinate system.

Acoustic particle velocities are defined as small amplitude motions of constant volume fluid particles (each particle having unvarying fluid properties) about some equilibrium position. Acoustic pressure is defined as the instantaneous pressure at a point, minus the hydrostatic pressure at that point. In cartesian coordinates, time-harmonic acoustic planewaves, which have wavefronts propagating in the direction of acoustic wavevector $-\bar{k}$ (by convention the acoustic wavenumber has been defined to point from the origin towards the source), can be characterized by acoustic pressure or by acoustic particle velocity. Thus,

$$p(\bar{r},\omega) = Pe^{i(\bar{k}\cdot\bar{r}+\omega t+\phi_p)},$$

(1)

$$v_x(\bar{r},\omega) = V_x e^{i(\bar{k}\cdot\bar{r}+\omega t+\phi_x)},$$

(2)

$$v_y(\bar{r},\omega) = V_y e^{i(\bar{k}\cdot\bar{r}+\omega t+\phi_y)},$$

(3)

and

$$v_z(\bar{r},\omega) = V_z e^{i(\bar{k}\cdot\bar{r}+\omega t+\phi_z)},$$

(4)

where $\|\bar{k}\|(=\omega/c)$ is the acoustic wavenumber, with ω the circular frequency, c is the sound speed, $\bar{r}=[x,y,z]$ is the position vector, P is the amplitude of the sound wave pressure, and

V_x, V_y, V_z are the amplitudes of the component velocities in the x, y, and z directions, respectively. The complete vector field may be written as

$$\vec{v}^{(3)}(\vec{r},\omega) = v_x(\vec{r},\omega)\vec{n}_x + v_y(\vec{r},\omega)\vec{n}_y + v_z(\vec{r},\omega)\vec{n}_z, \tag{5}$$

and it is noted that the velocity vector $\vec{v}^{(3)}$ comprises all three vector components and is complex; i.e., it has complex-valued components $[v_x, v_y, v_z]$. The vectors $\{\vec{n}_x, \vec{n}_y, \vec{n}_z\}$ are mutually perpendicular unit vectors aligned as shown in figure 1. The elements of an uniaxis vector-sensing array measure only one of the velocity vector components, such as v_x, v_y, or v_z, while the multiaxis arrays measure two or more of these orthogonal vectors. For example,

$$\vec{v}^{(1)}(\vec{r},\omega) = v_y(\vec{r},\omega)\vec{n}_y, \tag{6}$$

and

$$\vec{v}^{(2)}(\vec{r},\omega) = v_x(\vec{r},\omega)\vec{n}_x + v_z(\vec{r},\omega)\vec{n}_z. \tag{7}$$

The superscript denotes the dimension of the velocity vector, biaxial vector sensors having a dimension of 2, triaxial a dimension of 3. Other combinations are, of course, possible and will be discussed shortly.
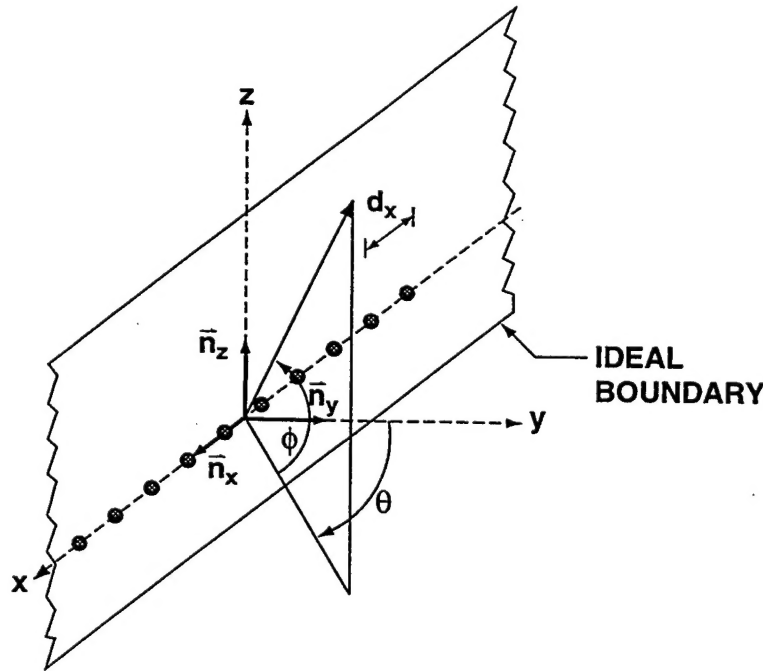
Figure 1. Array Coordinates and Geometry for an Equispaced
Line Array of Multiaxis Vector Sensors

3

It should be noted that, with collocated multiaxis vector sensors, the component phases, (ϕ_x, ϕ_y, ϕ_z), in equations (2), (3), and (4), may be referenced or calibrated in any manner relative to each other. That is, a single multiaxis-vector sensor could be used to determine whether propagating waves had clockwise or counterclockwise particle rotations by examining the differences in the component phases. A 90°-phase shift of a tangential component relative to the normal vector component would be indicative of a surface wave having clockwise particle rotations. This is an aside, but the relationship of the component phases may prove to be a useful property in subsequent investigations, such as in the use of vector sensors to cancel noise rather than detect signals. However, here the components of the vector sensors will be assumed to be in-phase, with the component phases set to zero. The harmonic time-dependence $\exp(i\omega t)$ of the acoustic pressure and particle velocities will be suppressed henceforth.

The spatial gradient of acoustic pressure and the particle velocities are related via Euler's linearized momentum equation. Namely, for harmonic waves,

$$\nabla p(\bar{r}) = -\rho_o \frac{\partial \bar{v}^{(3)}}{\partial t} = i\omega\rho_o(v_x(\bar{r})\bar{n}_x + v_y(\bar{r})\bar{n}_y + v_z(\bar{r})\bar{n}_z), \tag{8}$$

where the density of the fluid medium is denoted as ρ_o.

Now, if one considers a first-order Taylor series expansion of acoustic pressure about some point defined by the position vector $\bar{r}_o$, then,

$$p(\bar{r}) \cong p(\bar{r}_o) + \nabla p(\bar{r}_o) \cdot (\bar{r} - \bar{r}_o)$$

$$= p(\bar{r}_o) + i\omega\rho_o(v_x(\bar{r}_o)\bar{n}_x + v_y(\bar{r}_o)\bar{n}_y + v_z(\bar{r}_o)\bar{n}_z) \cdot (\bar{r} - \bar{r}_o), \tag{9}$$

where equation (8) has been substituted for the gradient in equation (9) and $\bar{r} - \bar{r}_o = (x - x_o)\bar{n}_x + (y - y_o)\bar{n}_y + (z - z_o)\bar{n}_z$. D'Spain remarked on this expansion, noting that the simultaneous measurement of acoustic pressure and particle velocity at a single point is equivalent to measuring the acoustic pressure in a volume of space about the measurement point. Therefore, a single multiaxis-vector sensor may be considered similar to a small (in terms of an acoustic wavelength) volumetric array of scalar pressure sensors, and a line array of multiaxis-vector sensors is equivalent to a line array of discrete volumetric pressure-sensing elements. However, the accuracy of the above expansion, since it is truncated to first order, decreases with increasing volumetric radius, $R = \|\bar{r} - \bar{r}_o\|$. This implies that the ability of equation (9) to correctly measure the acoustic pressure in a given volume of space is dependent on the acoustic wavelength. Comparing the ratio of the second-order Taylor series term (not shown) to the first-order term given in equation (9) indicates that the truncated expansion is valid for a volumetric radius less than approximately one-third of an acoustic wavelength.

Pressure-gradient hydrophones can measure the quantity ∇p as well by measuring the phase difference of a planewave between two spatially separated hydrophones. The separation distance must increase, in order to obtain an accurate estimate of the gradient, with increasing wavelength. At low frequencies, the separation distances required for pressure-gradient hydrophones are often too large to be feasible for array applications.

4

AMPLITUDE RESPONSE OF VECTOR SENSORS

The assumed geometry of an equispaced linear array of vector sensors is shown in figure 1. For the baffle configuration, the sensors lie in the xz-plane and are bounded by a semi-infinite acoustic medium for y > 0. The baffle here is assumed ideal; i.e., perfectly rigid in the case of an array of pressure sensors and entirely pressure release, for each component, in the case of an array of vector sensors. In equation (1), P is defined as the amplitude or angular sensitivity of the pressure sensor for angular coordinates, (θ,ϕ), where θ is defined as the azimuthal angle and ϕ the elevation angle. For half-omnidirectional element sensitivity on a rigid baffle

$$P(\theta,\phi) = \begin{cases} 2 & for -90° \leq \theta, \phi \leq 90° \\ 0 & otherwise \end{cases}. \tag{10}$$

It is assumed that each orthogonal component of a vector sensor has an amplitude response or element sensitivity which is proportional to the cosine of the angle between the planewave incidence arrival direction and each component normal (the component's maximum response axis). This assumption is based upon elementary solutions to the wave equation at the boundary of an ideal pressure release surface. The component normals are, for the simple line array configuration under investigation, equivalent to the unit normals, $\{\bar{n}_x, \bar{n}_y, \bar{n}_z\}$, as defined in figure 1.

The wavevector describing the orientation of the arrival of the incident planewave, shown in figure 2, is denoted $\vec{k}$ with components $[k_x, k_y, k_z]$. Figure 2 also depicts the conical angle Θ_y, as in equation (16), left-hand side, formed between y-unit normal, $\bar{n}_y$, and the arrival direction.
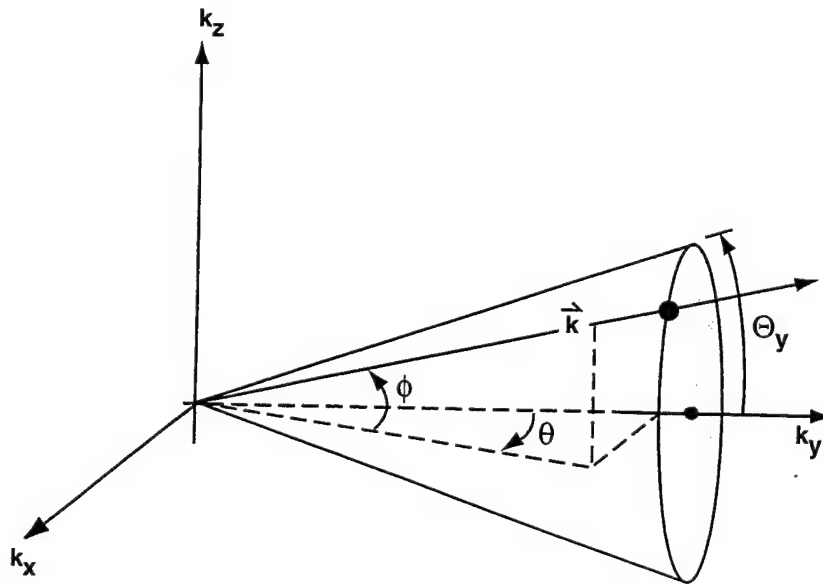
Figure 2. Angular Coordinates Used to Define Incident Direction of Acoustic Planewave at Wavevector $\bar{k}$

From figure 1 then,

$$k_x = \|\bar{k}\| \sin(\theta)\cos(\phi), \tag{11}$$

$$k_y = \|\bar{k}\| \cos(\theta)\cos(\phi), \tag{12}$$

and

$$k_z = \|\bar{k}\| \sin(\phi). \tag{13}$$

The angle formed between the vectors $\bar{k}$ and $\{\bar{n}_x, \bar{n}_y, \bar{n}_z\}$ can be determined via their dot product. Hence, cosine angular dependence yields

$$V_j(\theta,\phi) = \begin{cases} 2\cos(\Theta_j) & \textit{for } -90° < \theta, \phi < 90° \textit{ and } j = x, y, z \\ 0 & \textit{otherwise} \end{cases}, \tag{14}$$

where

$$\cos(\Theta_x) = \cos(\phi)\sin(\theta), \tag{15}$$

$$\cos(\Theta_y) = \cos(\phi)\cos(\theta), \tag{16}$$

and

$$\cos(\Theta_z) = \sin(\phi). \tag{17}$$

The factor of 2 in equation (14) is due to the assumption of an ideal surface, thereby doubling the signal amplitude for all angles of incidence. Thus, a baffled triaxial vector sensor can be expressed as

$$\bar{v}^{(3)}(\theta,\phi,\bar{r}_o) = 2\{\cos(\Theta_x)e^{ik_x x_o}\bar{n}_x + \cos(\Theta_y)e^{ik_y y_o}\bar{n}_y + \cos(\Theta_z)e^{ik_z z_o}\bar{n}_z\}, \tag{18}$$

with the velocity vector dependence on azimuthal and elevation angles now explicitly indicated.

Another illustration of the conical angles associated with each vector component is given in figure 3. Here the amplitude response of the vector components, v_x, v_y, and v_z, on an ideal boundary, are characterized. In the free field, of course, the vector sensor responses are simply reduced by one-half and extended over all acoustic space ($-180° < \theta < 180°$, $-90° < \phi < 90°$).

The amplitude response of a half-omnidirectional pressure sensor, given by equation (10), is shown as a gray scale image in figure 4. In all of these images, the darker regions correspond to minima and bright to maxima, and for figures 4 through 12, the gray scale varies from zero to a maximum value of 2, shown as white. The abscissa is azimuthal angle θ from -90° to +90°; the elevation angle is shown on the ordinate over the same angular region. For illustration, in figure 4 only, the half-omnidirectional critical angle was set to $\pm 89°$. As indicated, the amplitude response of a half-omnidirectional pressure sensor is essentially uniform over the entire acoustic domain of interest.

Figure 5 shows the amplitude response of a uniaxial velocity sensor aligned along the y-axis, or the amplitude V_y of the velocity component v_y.
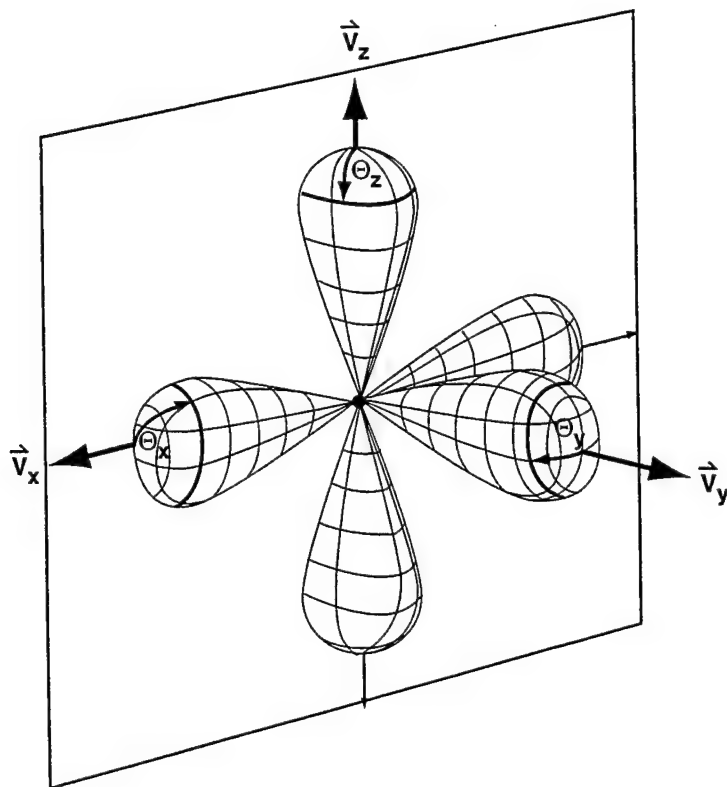
Figure 3. Triaxial Vector Sensor Element Response on an Ideal Boundary Showing Conical Angles Θ_x, Θ_y, Θ_z
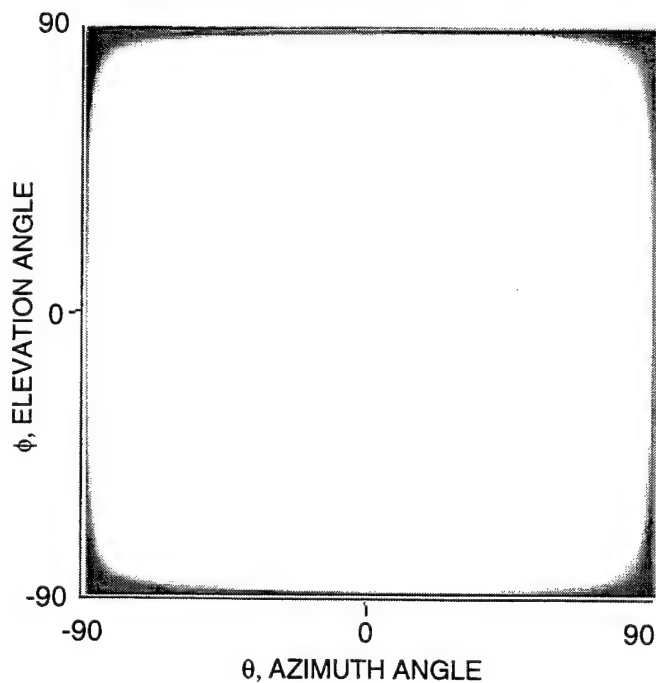
Figure 4. Amplitude Response of a Half-Omnidirectional Pressure Sensor on a Rigid Boundary
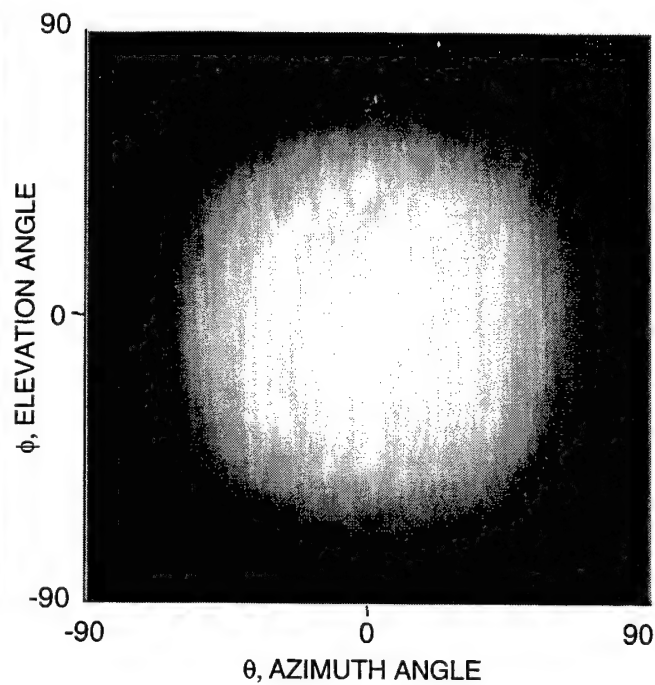
Figure 5. Amplitude Response of the v_y-Component of a Uniaxial-Vector Sensor on an Ideal Pressure Release Boundary

A cross-section of this element response, showing the cosine angular dependence, is given in figure 6. The amplitude of V_y is reduced by one-half at $\pm 60°$. Responses for V_x and V_z are shown in figures 7 and 8. For illustration, both of the amplitude lobes of V_x and V_z are shown positive; the polarity is suppressed. Figures 9, 10, and 11 show the element response combinations possible from a biaxial vector sensor. In figure 9, the vector magnitude of the amplitudes of V_x and V_y are shown. Notice, in figure 10, that a biaxial sensor which measures only velocities in the xz-plane produces a null at broadside steerings ($\theta = 0°$).

The element response for a triaxial vector sensor is given in figure 12, and as with the half-omnidirectional-pressure sensor, the element response is uniform for all elevation and azimuth arrival angles. Hence, the magnitude of a triaxial vector sensor yields an element response equivalent to a scalar pressure sensor. Some may then question what benefit, in terms of element sensitivity, triaxial vector sensors have over pressure-sensors. One notable benefit is described in the following section, namely, the ability to steer a single vector sensor in the planewave arrival direction.
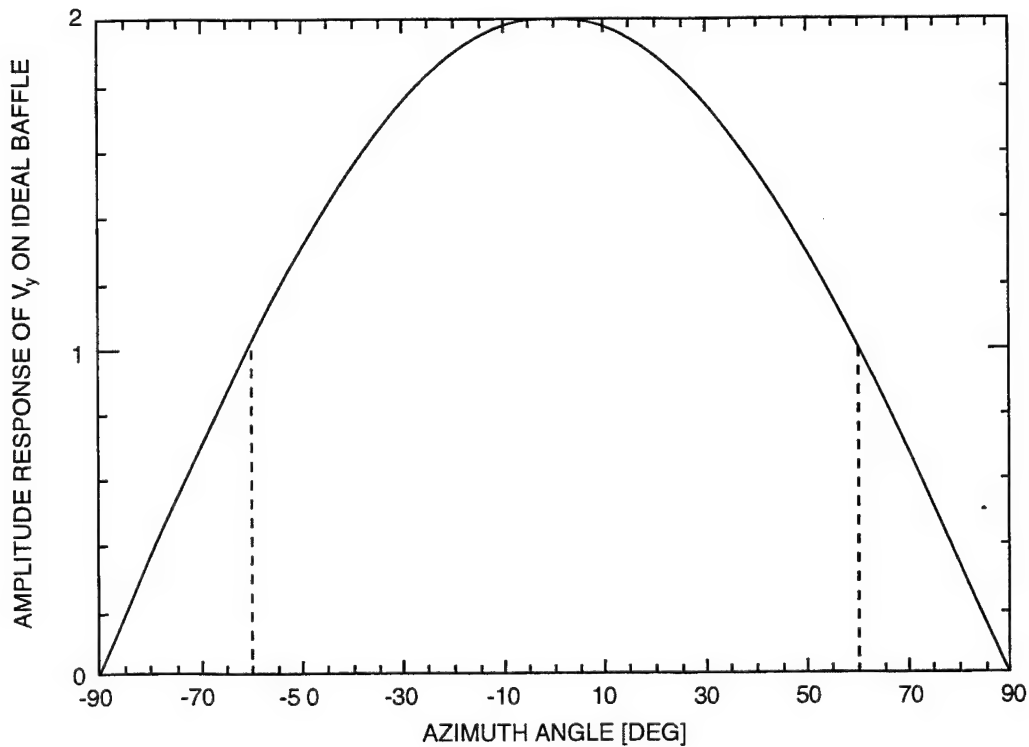
Figure 6. Cross Section of the Amplitude Response of the v_y-Component of a Uniaxial Vector Sensor versus Azimuth Angle ($\phi = 0°$)
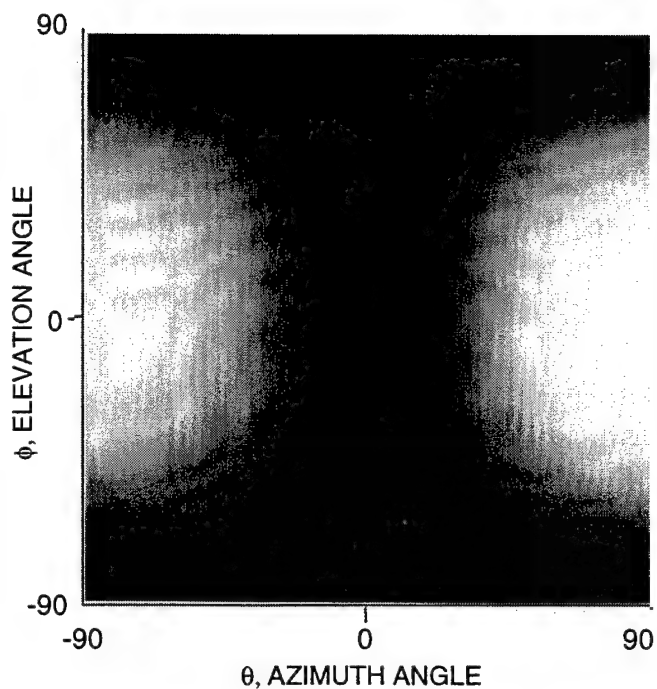
Figure 7. Amplitude Response of the
v_x-*Component of a Uniaxial Vector Sensor*
on an Ideal Pressure Release Boundary
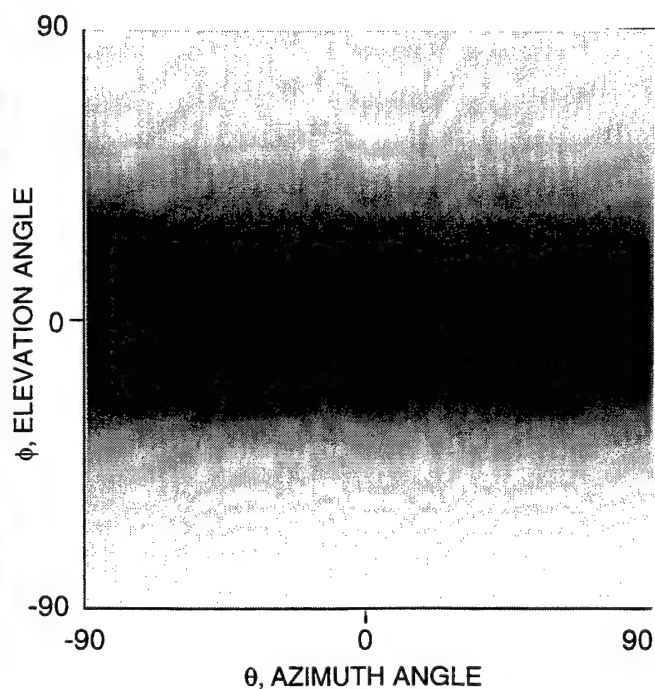
Figure 8. Amplitude Response of the
v_z-*Component of a Uniaxial Vector Sensor*
on an Ideal Pressure Release Boundary
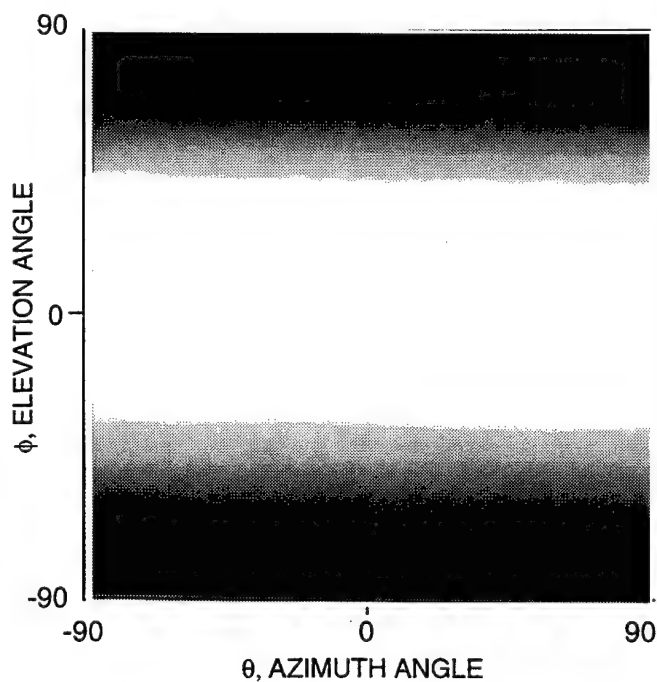
Figure 9. Magnitude of the v_x- *and* v_y-
Components of a Biaxial Vector Sensor on
an Ideal Pressure Release Boundary
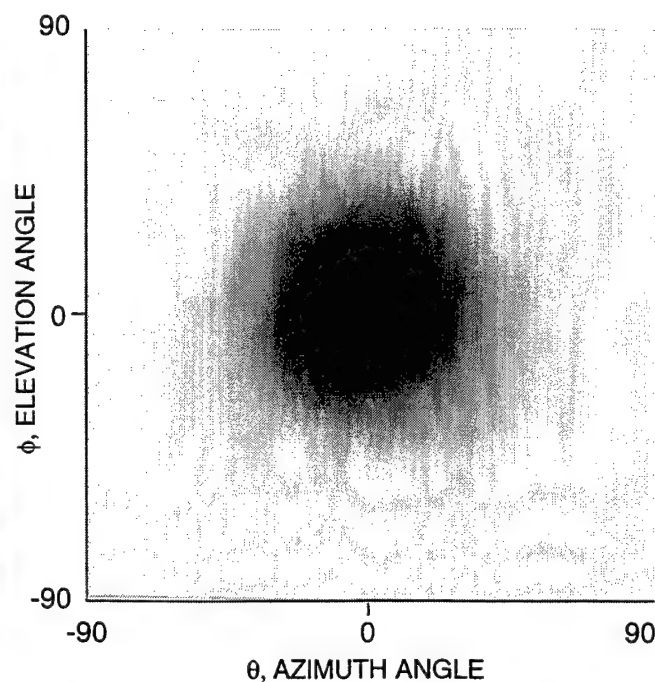
Figure 10. Magnitude of the v_x- *and* v_z-
Components of a Biaxial Vector Sensor on
an Ideal Pressure Release Boundary

9
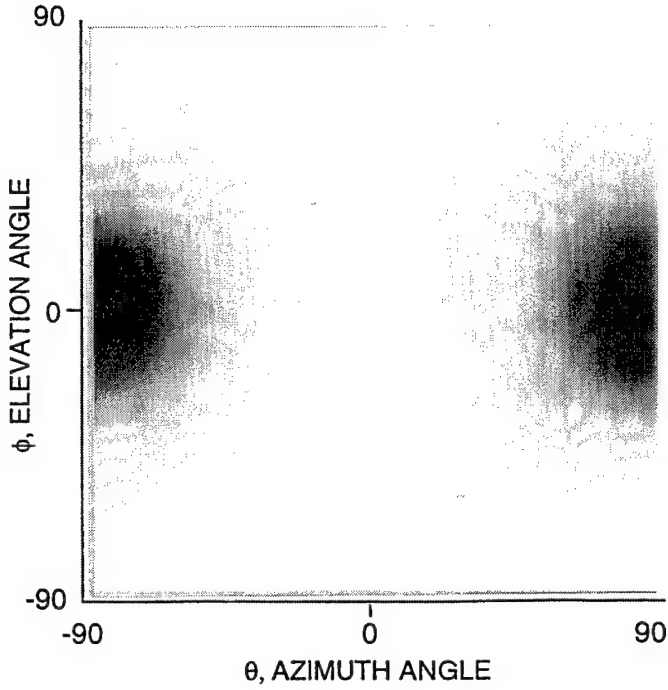
Figure 11. Magnitude of the v_y- and v_z-Components of a Biaxial Vector Sensor on an Ideal Pressure Release Boundary
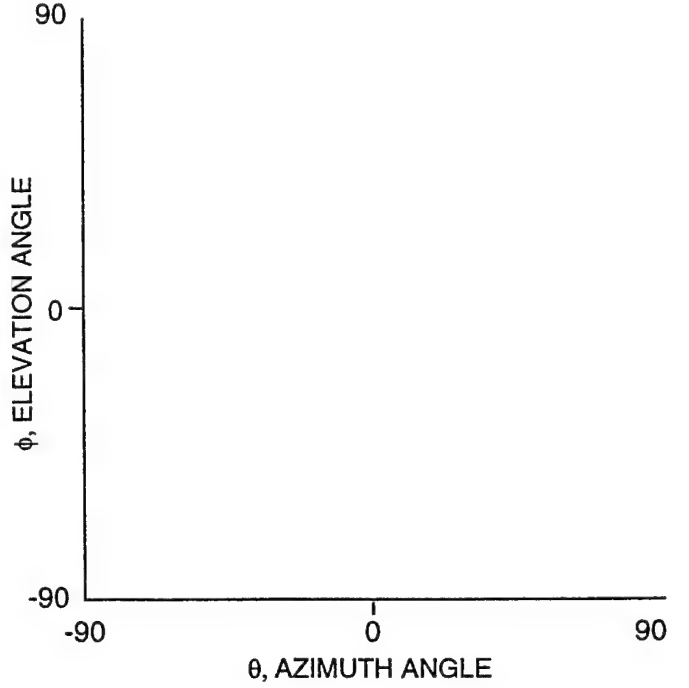
Figure 12. Magnitude of the v_x-, v_y-, and v_z-Components of a Triaxial Vector Sensor on an Ideal Pressure Release Boundary

BEAMFORMING A SINGLE VECTOR SENSOR

It is possible to form a broad acoustic beam, which is steered in the direction of the incident wavevector, $\vec{k}$, using a single triaxial vector sensor. A biaxial sensor may be steered as well, but only in one angle, such as azimuth.

Consider the vector-sensor response given in equation (18), with the sensor located at the origin,

$$\vec{v}^{(3)}(\theta, \phi, \bar{0}) = 2\{\cos(\Theta_x)\bar{n}_x + \cos(\Theta_y)\bar{n}_y + \cos(\Theta_z)\bar{n}_z\}. \tag{19}$$

Then, as outlined in reference 4, the dot product of the normalized velocity field vector at the angle at which the element is steered (θ_s, ϕ_s), and the velocity vector at arrival angle (θ, ϕ), may be taken, yielding

$$\frac{\vec{v}^{(3)}(\theta_s, \phi_s, \bar{0}) \cdot \vec{v}^{(3)}(\theta, \phi, \bar{0})}{\left\|\vec{v}^{(3)}(\theta_s, \phi_s, \bar{0})\right\| \left\|\vec{v}^{(3)}(\theta, \phi, \bar{0})\right\|} = g^{(3)}(\theta_s, \phi_s, \theta, \phi)$$

$$= \cos(\phi_s)\cos(\phi)\cos(\theta - \theta_s) + \sin(\phi_s)\sin(\phi). \tag{20}$$

The product $g^{(3)}(\theta_s, \phi_s, \theta, \phi)$ reaches a maximum of unity when $(\theta_s, \phi_s) = (\theta, \phi)$. For a biaxial sensor, measuring the components v_x and v_y, the steered element response is

10

$$g^{(2)}(\theta_s, \theta) = \cos(\theta - \theta_s). \tag{21}$$

Figures 13 and 14 present the amplitude response and the associated beam pattern (log of the squared amplitude response) of a single triaxial vector sensor steered to 45° azimuth and 30° elevation. The amplitude is not symmetrical about the steered direction, i.e., the beamwidth is broader in azimuth than elevation. This is caused by the cosine directionality of each component amplitude, the summed response being a combination of cosines.

Shown in figure 15 are beam patterns for a triaxial element steered to 0° azimuth and various elevation angles. In elevation, the power in each element beam is reduced by one-half at $\pm 60°$, as predicted for cosine directivity and shown previously. The half-power beamwidth does, however, vary with other element steerings. For example, figure 14 illustrates the beam pattern for the amplitude response given in figure 13. Here, the half-power beamwidth occurs when the arrival angles are such that $g^{(3)}(45°, 30°, \theta, \phi)$ equals one-half. All of the element beamwidths are frequency-independent.
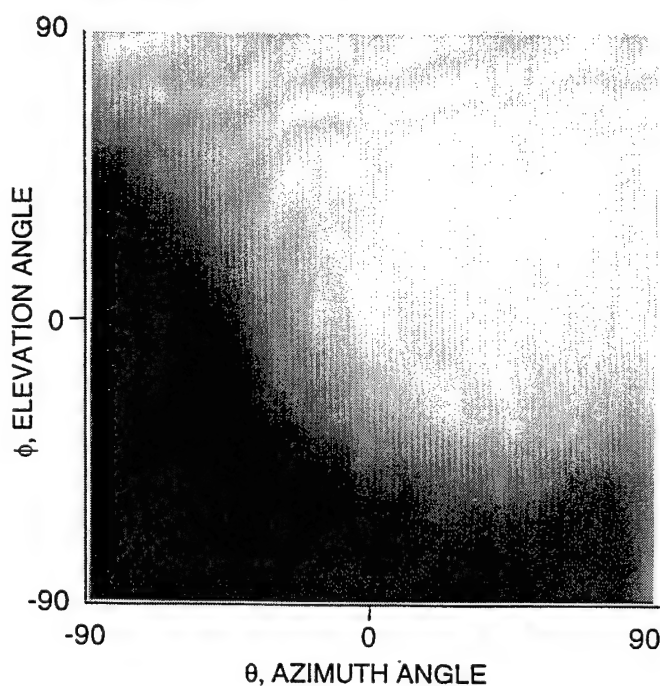
Figure 13. Amplitude Pattern of a Single Triaxial Vector Sensor Steered to 45° Azimuth and 30° Elevation
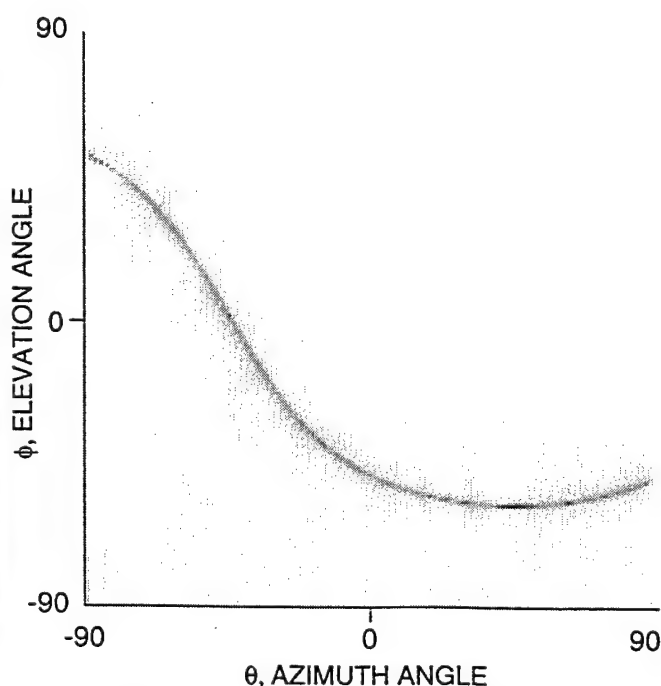
Figure 14. Beam Pattern of a Single Triaxial Vector Sensor Steered to 45° Azimuth and 30° Elevation

With additional sensors, the accuracy of the estimation of the signal arrival angle from steering individual sensors would improve – assuming the steering errors at each sensor were uncorrelated. Hence, one could consider steering a horizontal line array in elevation by averaging over each single-element beam response. The averaging process would provide little resolution improvement, so the directivity in elevation would be limited, as indicated in figure 15. The elements in the horizontal direction can, of course, be phase delayed, weighted, and summed, which would provide azimuthal resolution. Thus, one possible array beamforming procedure is to steer each vector-sensor element in the direction of the estimated arrival angle and beamform the resulting responses conventionally.

11
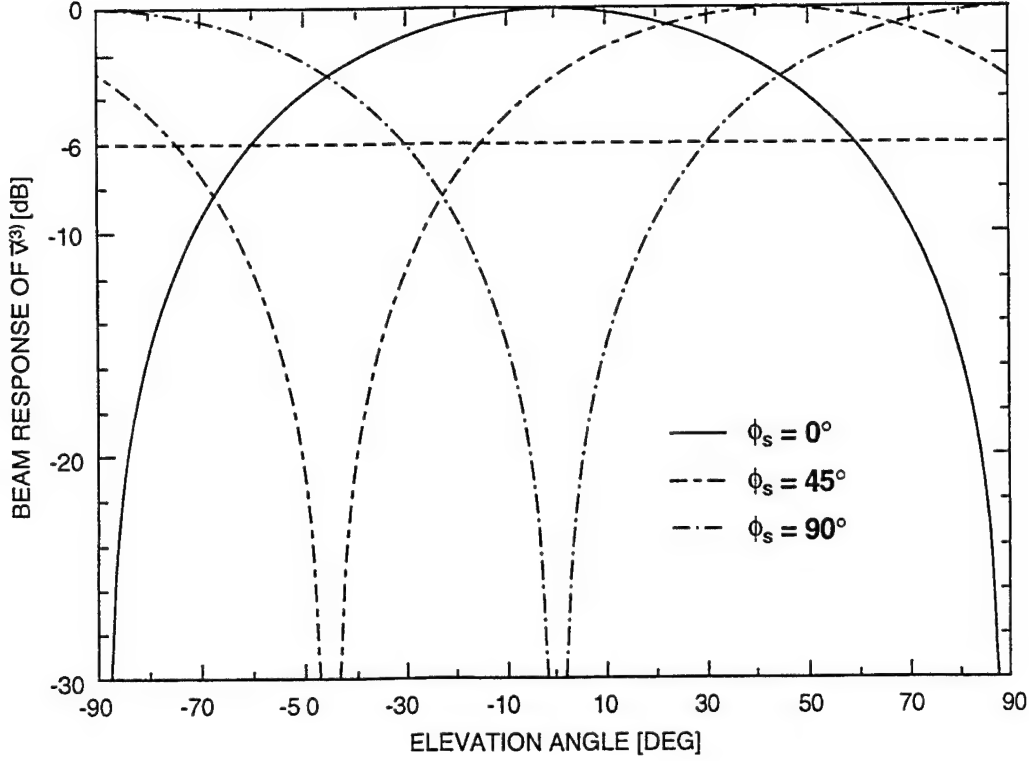
Figure 15. Beam Pattern in Elevation of a Single Triaxial Vector Sensor Steered to Elevation Angles of 0°, 45°, and 90°

BEAMFORMING AN ARRAY OF VECTOR SENSORS

The line array depicted in figure 1 consists of ten elements, with interelement spacing d_x. This array configuration allows for element-to-element phase variations along the x-axis only. That is, for a fixed incident planewave, the phase at each element is constant with respect to the y- and z-axis and varies only with respect to the x-axis. Therefore, phase can be delayed (or the array can be steered) only by delaying phase components along the x-axis, such as is the case with scalar pressure sensors. This is fundamental; with conventional array beamforming, regardless of the type of array (line, planar, or volumetric), the phase delays are no different for a scalar or vector-sensing array.

A possible approach to beamforming an array of vector sensors would be to delay, weight, and sum the velocity components from each triaxial vector sensor separately. Thus, for the ideal baffle configuration

$$\bar{v}_N^{(3)}(\theta,\phi) = 2\sin(\theta)\cos(\phi)\sum_{n=1}^{N} w_n^{(x)} e^{i(\bar{k}-\bar{k}_s)\cdot\bar{r}_n}\bar{n}_x + 2\cos(\theta)\cos(\phi)\sum_{n=1}^{N} w_n^{(y)} e^{i(\bar{k}-\bar{k}_s)\cdot\bar{r}_n}\bar{n}_y$$

$$+ 2\sin(\phi)\sum_{n=1}^{N} w_n^{(z)} e^{i(\bar{k}-\bar{k}_s)\cdot\bar{r}_n}\bar{n}_z, \tag{22}$$

12

where the amplitude shading coefficients, $w_n^{(x)}, w_n^{(y)}, w_n^{(z)}$, are arbitrary. The wavevector $\bar{k}$, defined by equations (11), (12), and (13), corresponds to the arriving acoustic planewave, and $\bar{k}_s$ is the wavevector to which the array is steered. It is also noted that the exponential functions in equation (22) may be written more explicitly as

$$e^{i(\bar{k}-\bar{k}_s)\cdot\bar{r}_n} = \exp\left[i\frac{\omega}{c}\left\{x_n\alpha(\theta,\phi) + y_n\beta(\theta,\phi) + z_n\gamma(\theta,\phi)\right\}\right], \tag{23}$$

where

$$\alpha(\theta,\phi) = \cos(\phi)\sin(\theta) - \cos(\phi_s)\sin(\theta_s), \tag{24}$$

$$\beta(\theta,\phi) = \cos(\phi)\cos(\theta) - \cos(\phi_s)\cos(\theta_s), \tag{25}$$

and

$$\gamma(\theta,\phi) = \sin(\phi) - \sin(\phi_s). \tag{26}$$

One may then be tempted to simply take the norm (or length of the weighted sum of all the vector components) of $\bar{v}_N^{(3)}$ in equation (22) as a means to process the vector components. That is, the norm may be written as

$$B^{(3)}(\theta,\phi) = \sqrt{\left(\sum_{n=1}^{N} w_n^{(x)} v_{xn}\right)^2 + \left(\sum_{n=1}^{N} w_n^{(y)} v_{yn}\right)^2 + \left(\sum_{n=1}^{N} w_n^{(z)} v_{zn}\right)^2},$$

where $v_{xn} = V_x \exp\{i(\bar{k}-\bar{k})\cdot\bar{r}_n\}$, etc. Clearly, this approach results in taking the square-root of the sum of the squared vector velocity components; this is a nonlinear *ad hoc* processing technique that should be avoided.

Another approach to array beamforming, as previously described, would be to steer *each* vector sensor in equation (22) towards the source, and then obtain the squared magnitude of the resulting expression. That is, form the inner product of the summed velocities, $\bar{v}_N^{(3)}$, with a steered vector of unit amplitude and take the magnitude-squared of the product. If it is assumed that the weighting of each component of every vector sensor is identical, i.e.,

$$w_n^{(x)} = w_n^{(y)} = w_n^{(z)} = w_n,$$

and, for the line array in figure 1, $\bar{r}_n = [x_n, 0., 0.]$, then this approach yields

13

$$B^{(3)}(\theta, \phi) = \left\| \vec{v}_N^{(3)}(\theta, \phi) \cdot \vec{v}^{(3)}(\theta_s, \phi_s) \right\|^2$$

$$= 4g^{(3)}(\theta_s, \phi_s, \theta, \phi)^2 \left| \sum_{n=1}^{N} w_n \exp\left(i\frac{\omega}{c} x_n \alpha(\theta, \phi)\right) \right|^2. \tag{27}$$

Similarly,

$$B^{(2)}(\theta, \phi) = 4\{g^{(2)}(\theta_s, \theta)\cos(\phi)\}^2 \left| \sum_{n=1}^{N} w_n \exp\left(i\frac{\omega}{c} x_n \alpha(\theta, \phi)\right) \right|^2. \tag{28}$$

There is no equivalent expression for a <u>uniaxis</u> vector-sensing array since such elements cannot be steered in azimuth or elevation. Therefore, the uniaxial beam response (for measuring the vector component v_y) would be written simply as

$$B^{(1)}(\theta, \phi) = \left\| \vec{v}^{(1)}(\theta, \phi) \right\|^2 = 4\cos^2(\theta)\cos^2(\phi) \left| \sum_{n=1}^{N} w_n \exp\left(i\frac{\omega}{c} x_n \alpha(\theta, \phi)\right) \right|^2. \tag{29}$$

As an aside, it is noted that the summations given above can be written in a more compact form for certain array configurations. For example, with uniform-shading weights, and equal element array spacing, Lagrange's trigonometric identity gives

$$\sum_{n=1}^{N} w_n \exp\left(i\frac{\omega}{c} x_n \alpha(\theta, \phi)\right) = \sin(NA)/\sin(A) \quad \text{if } x_1 = -x_N, \tag{30}$$

where

$$A = \pi \frac{d_x}{\lambda} \alpha(\theta, \phi).$$

This second approach to beamforming, however, may be limited in its capability. The restriction of weighting values to be essentially the direction cosines and constant from element to element disallows emphasis of some element outputs over others and it imposes the same relative weighting to the three velocity components.

A more general <u>linear</u> processing technique would form the inner product of the velocity at each element location with an arbitrary element weighting vector, $\vec{w}_n^{(3)}$, which now may vary at each element array location. The resulting scalar field may then be delayed and summed in a conventional manner. Thus, in general,

$$B^{(3)}(\theta, \phi) = \left| \sum_{n=1}^{N} \vec{w}_n^{(3)} \cdot \vec{v}_n^{(3)} e^{i(\vec{k} - \vec{k}_s) \cdot \vec{r}_n} \right|^2, \tag{31}$$

14

$$B^{(3)}(\theta,\phi) = \left| \sum_{n=1}^{N} \bar{w}_n^{(3)} \cdot \bar{v}_n^{(3)} \, e^{i(\bar{k}-\bar{k}_s)\cdot\bar{r}_n} \right|^2, \tag{31}$$

and for the line array,

$$B_L^{(3)}(\theta,\phi) = \left| \sum_{n=1}^{N} \left(w_n^{(x)} V_x + w_n^{(y)} V_y + w_n^{(z)} V_z \right) \exp\left(i\frac{\omega}{c} x_n \alpha(\theta,\phi)\right) \right|^2. \tag{32}$$

Hence, the result here is a linearly-weighted combination of all three measured velocity components. That is, this approach yields the square of the sum of the weighted velocity components. A special case of the general weighting vector, $\bar{w}_n^{(3)}$, would be constant direction cosine weights.

The most general linear processing, likely only realizable in a free-field environment, would be to augment equation (31) with a measurement of acoustic pressure. Processing all 4N measured quantities, i.e., pressure and three velocity components at each element location, yields

$$B^{(pv)}(\theta,\phi) = \left| \sum_{n=1}^{N} (\bar{w}_n^{(3)} \cdot \bar{v}_n^{(3)} + w_p P_n) \, e^{i(\bar{k}-\bar{k}_s)\cdot\bar{r}_n} \right|^2. \tag{33}$$

There are now 4N degrees of freedom to manipulate, in order to maximize some measure of performance, such as the array output signal-to-noise ratio. These 4N degrees of freedom are the N pressure weights $\{w_p\}$ and the N velocity weights for each orthogonal direction, namely, $\{w_n^{(x)}\}$, $\{w_n^{(y)}\}$, $\{w_n^{(z)}\}$ for $1 \le n \le N$. This increased number of degrees of freedom should allow for considerably improved performance relative to pressure-alone processing.

For reference, the power response for a line array of baffled scalar pressure sensors is

$$B^{(p)}(\theta,\phi) = 4 \left| \sum_{n=1}^{N} w_n \exp\left(i\frac{\omega}{c} x_n \alpha(\theta,\phi)\right) \right|^2. \tag{34}$$

Hence, from equation (27), it is seen that the acoustic power from a uniformly-weighted line array of pressure sensors is equivalent to that from an array of triaxial vector sensors at the array's maximum response axis. At elevation angles, $\phi = \pm\pi/2$, the uniaxial (equation (29)) and biaxial (equation (28)) line arrays considered here receive no power, and the uniaxial vector-sensing array also has a null response at azimuthal endfire. Such is not the case for the half-omnidirectional pressure-sensing array.

15

NUMERICAL RESULTS

COMPARISON OF BEAM PATTERNS

The beam pattern of an ideally-baffled 10-element triaxial vector-sensing line array, with half-wavelength element separations and steered to broadside, is shown in figure 16, which employs a gray scale from -30 dB to 0 dB. For comparison, figure 17 illustrates the beam pattern from a pressure-sensing array steered to broadside. For broadside steering, the beam patterns from both array types are alike. The triaxial vector sensors provide greater vertical directivity, due to the cosine dependence, than the half-omnidirectional pressure sensors. Figure 18 compares the primary sidelobe structure, in azimuth, of both arrays. Again, the cosine angular dependence of the vector sensor lowers the sidelobe levels, the reduction increasing as the azithumal arrival angle increases. This overall sidelobe reduction produces an insignificant broadening of the azimuthal mainbeam width.
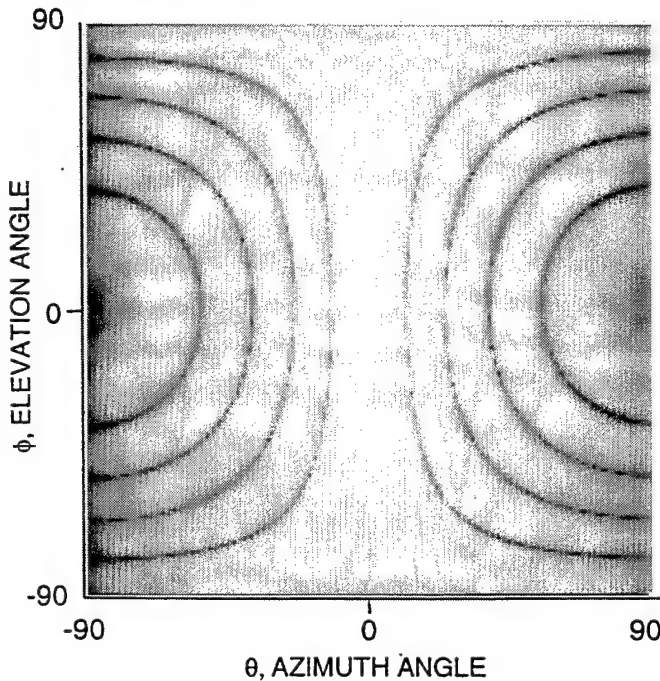
Figure 16. Beam Pattern at Broadside of a Linear 10-Element Triaxial Vector-Sensing Array Having Uniform Shading Weights
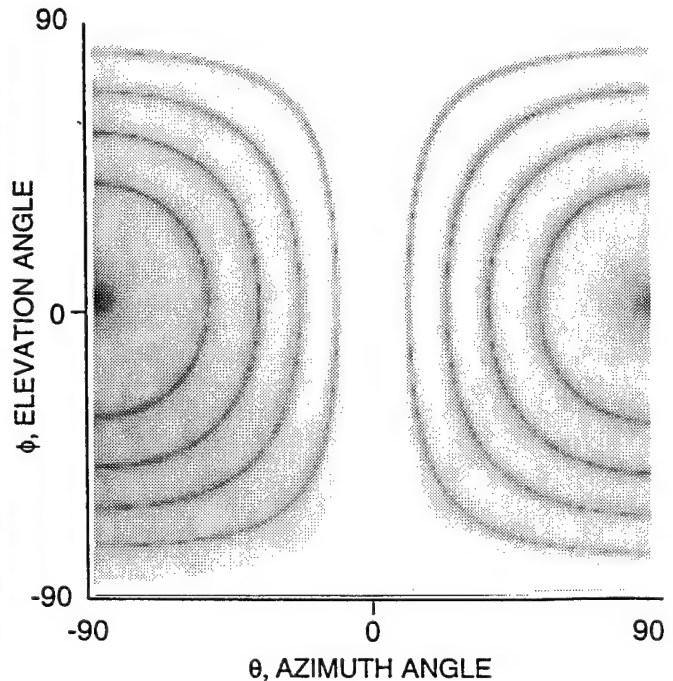
Figure 17. Beam Pattern at Broadside of a Linear 10-Element Pressure-Sensing Array Having Uniform Shading Weights

The differences in vector- and scalar-array patterns become more apparent when the array is steered to oblique angles of incidence. For example, figure 19 illustrates the beam pattern produced from a triaxial vector-sensing array steered to 45° azimuth and 30° elevation. Referring back to figure 14, it is clear that the array's beam pattern is the product of the steered element response and the array's response. The beam pattern from a pressure-sensing array is presented in figure 20. In both figures, the null structure of the array's response is identical, as indicated by equations (27) and (34). The differences seen are due to the inherent vector-sensor directionality and single-element steering of each vector sensor. Therefore, at oblique angles of incidence, a vector sensor may provide an increase in array directivity over that of a pressure-sensing array. This increase is quantified in the next section.

16
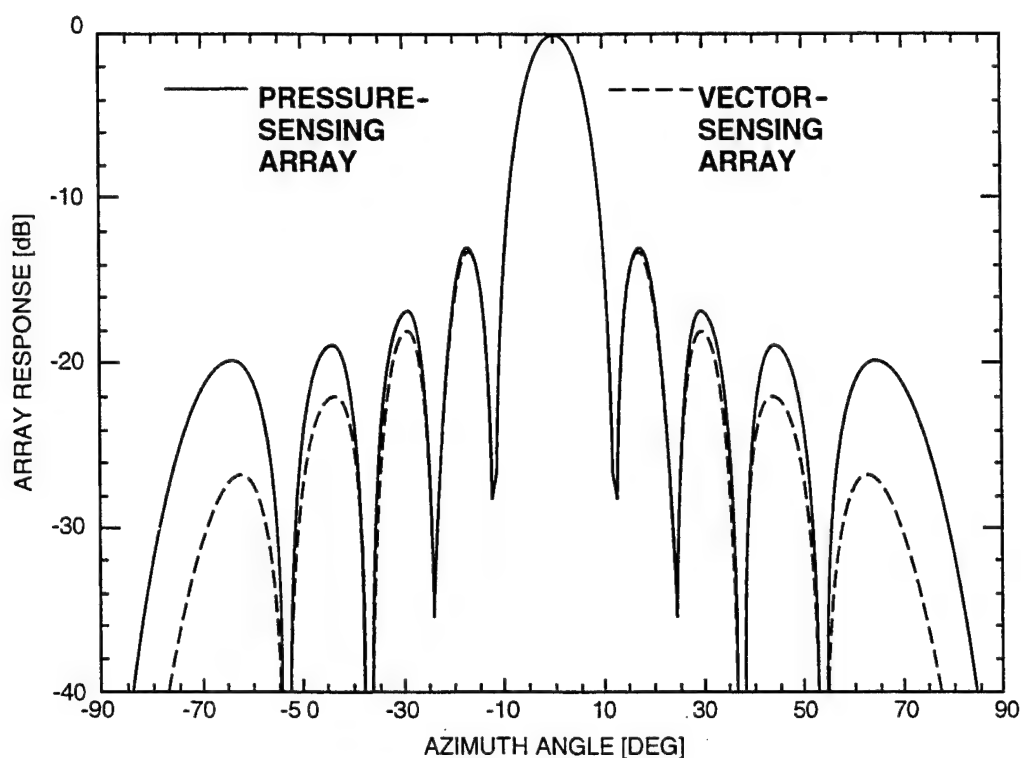
*Figure 18. Comparison of the Azimuthal Beam Pattern of
Vector- and Pressure-Sensing Arrays at Broadside*
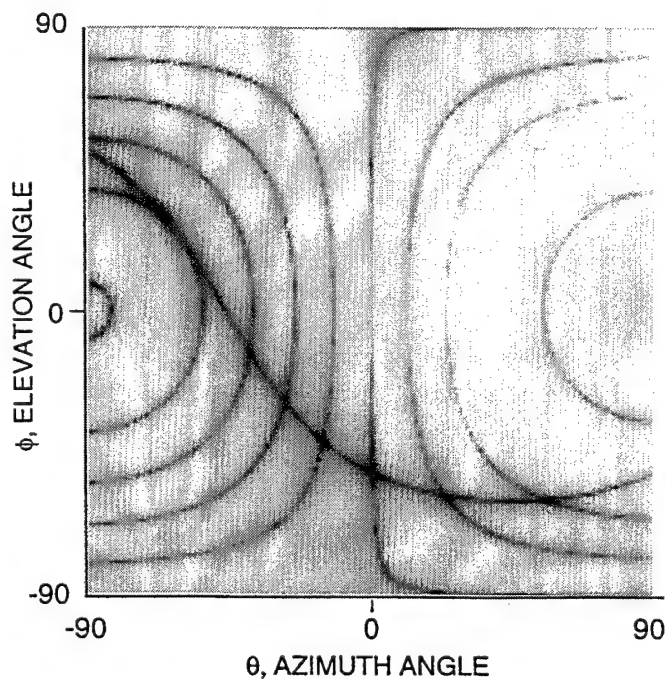
*Figure 19. Beam Pattern of a Linear
10-Element Triaxial Vector-Sensing Array
Having Uniform Shading Weights Steered to
45° Azimuth and 30° Elevation*
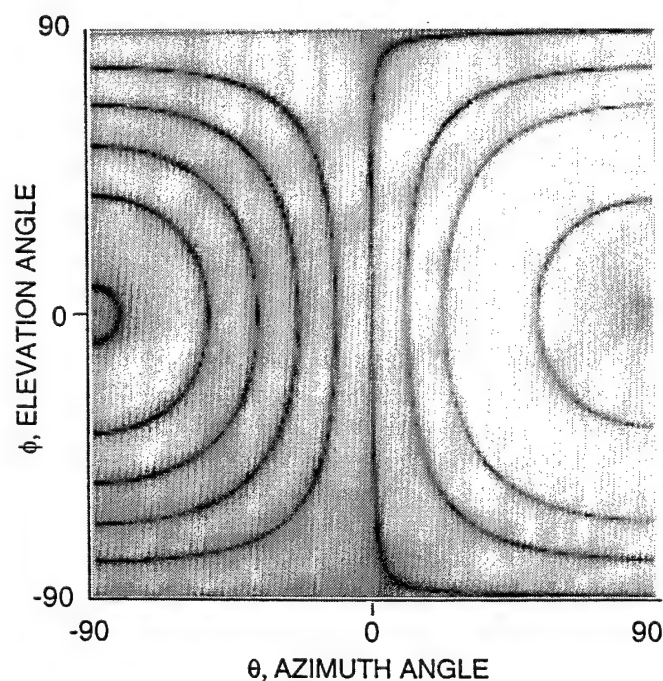
*Figure 20. Beam Pattern of a Linear
10-Element Pressure-Sensing Array Having
Uniform Shading Weights Steered to
45° Azimuth and 30° Elevation*

17

FREE-FIELD DIRECTIVITY CALCULATIONS

A comparison of free-field array directivity of a line array of scalar sensors detecting acoustic pressure and an array of vector sensors detecting acoustic particle motion in up to three orthogonal directions is presented here. Appendix A includes an analytical derivation for the directivity of some vector-sensing line arrays. The calculations presented here, though, were based on the derivative given in Appendix B. This derivation maximizes directivity by choosing array shading weights constrained to be real-valued, which maximize the array signal-to-noise ratio assuming a surrounding spherically isotropic noise field.

Figure 21 compares the maximum directivity index of an N-element pressure sensing line array to an uniaxial vector-sensing array which measures only the y-component of acoustic particle velocity. The elements of the arrays are equispaced at half-wavelength spacing and are aligned along the x-axis in the free field. The arrays have been steered to broadside ($\theta_s = \phi_s = 0°$) in figure 21 and endfire ($\theta_s = 90°$, $\phi_s = 0°$) in figure 22. Also shown in the figures is the directivity index for an array which measures both acoustic particle velocity and pressure.

For a planewave signal arriving at broadside, that is, along the y-axis, there would be no particle velocity in the x- or z-directions. Hence, for this array steering, there would be no additional directivity gains from measuring the velocities v_x or v_z. Similarly, for planewaves arriving at endfire, only the x-component of acoustic particle velocity is non-zero.

Since the directivity calculations are based on a half-wavelength equispaced line, a 10-element pressure-sensing array has a length of 5λ, for a directivity of 10 dB. Notice, in figure 21, that the uniaxial vector sensing array achieves 10 dB of directivity with half that number of elements and has a length of 2.5λ. The array that measures both pressure and velocity provides 10 dB of directivity at a length of only 1.5λ, and the total number of channels (i.e., 6) is still less than the number of elements on the pressure-sensing array.

The differences between the directivity gains shown in these figures is due to the orientation of the vector sensors with respect to the incident planewave. In figure 21, the difference in directivity between pressure sensing and vector sensing (v_y-component only) remains essentially constant with increasing array aperture. This is because the azimuthal beamwidth narrows, with increasing aperture, identically for the pressure and vector sensors. Hence, the gain shown is due to a constant difference between elevation beamwidths. The uniaxial vector sensor has a cosine element response, whereas the pressure sensor is assumed omnidirectional. In elevation, the directivity of the vector sensor is twice that of the pressure sensor. Hence, there is a constant difference of 3 dB.

In figure 22, the difference between the directivity index of the vector-sensing array and a pressure-sensing array diminishes with increasing array aperture. Again, the endfire beamwidth narrows identically for both the pressure- and vector-sensing arrays with increasing aperture. However, since the arrays are steered to endfire, the effect of the broad angular difference between the cosine and omnidirectional element response becomes negligible in comparison to the endfire beamwidth. That is, with increasing aperture, the directivity is determined entirely by the array beamwidth and is minimally influenced by the individual element response. This is a feature unique to endfire steerings.
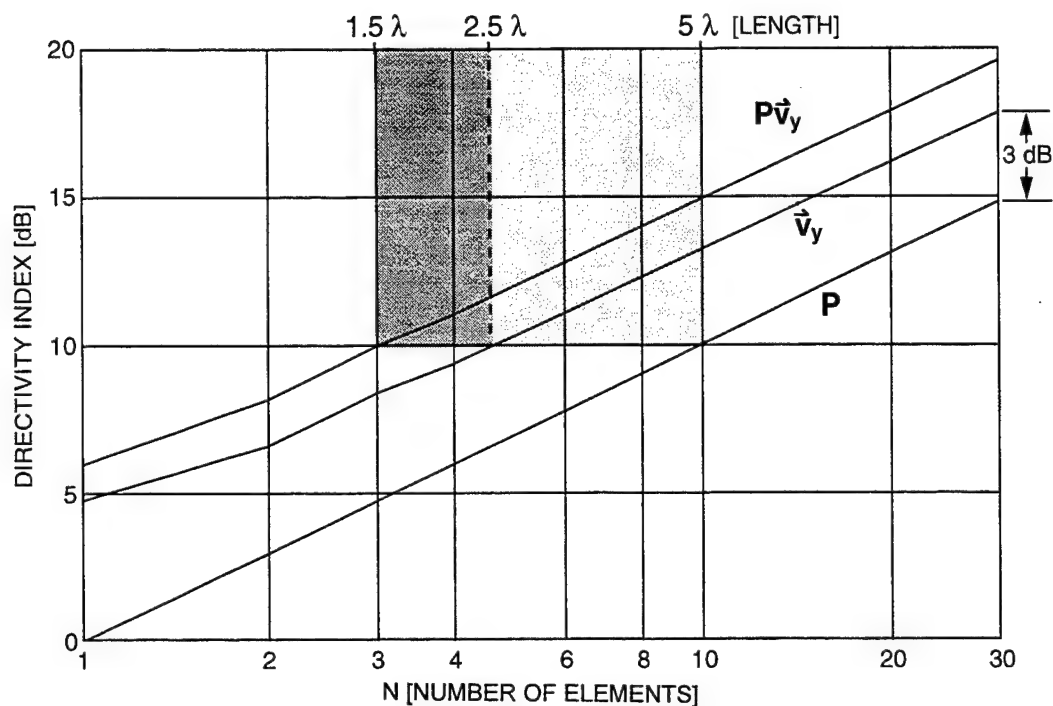
Figure 21. Maximum Directivity for an N-Element Equispaced Line Array at Broadside ($\theta_S = 0°$) Utilizing Optimal Real Weights
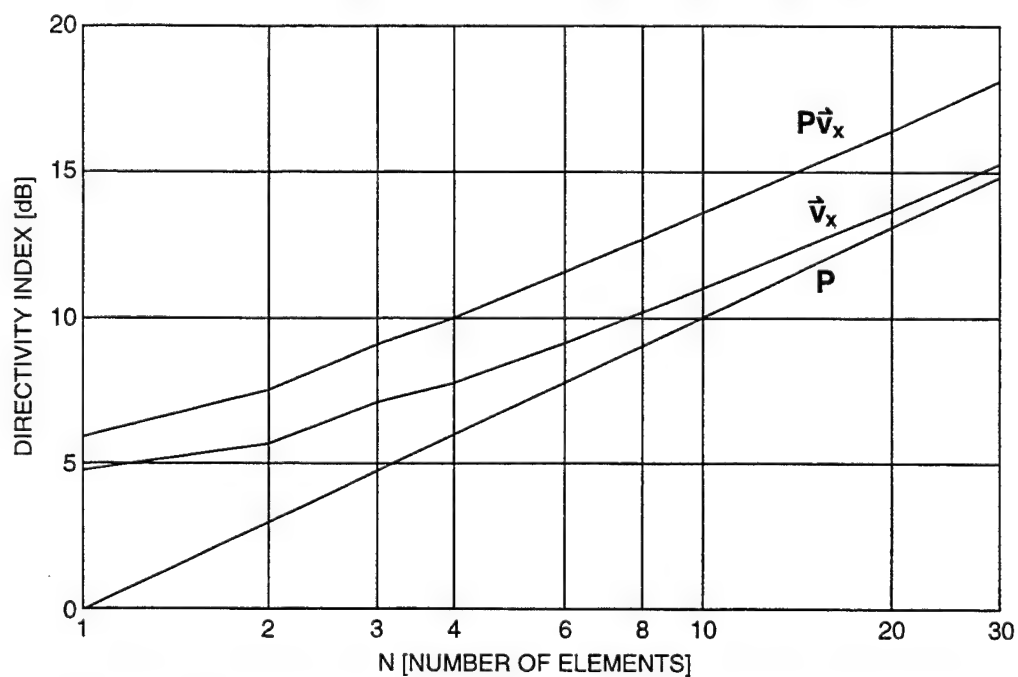
Figure 22. Maximum Directivity for an N-Element Equispaced Line Array at Endfire ($\theta_S = 90°$) Assuming Optimal Real Weights

19

Also shown is the directivity of an array that measures both acoustic pressure and particle velocity. Including the pressure increases the directivity for both array steerings and the increased gain appears to be directly proportional to the number of array elements, N. That is, the directivity factor can be expressed as $DF_{pv} = DF_v + N$, for optimal weightings at these steerings. This simple relationship does not appear to hold for general array steerings, as will be demonstrated in figures 23 through 25. Notice that, for a single element ($N = 1$) and for either array steerings, the uniaxis vector sensor provides a 4.8 dB gain over the omnidirectional pressure-sensing element. Measurement of both pressure and velocity yields a 6 dB gain. Appendix A provides a description of the source for these gains.

In figure 23, a comparison is made between the variation of directivity with azimuth for a pressure-sensing and vector-sensing line array. A 10-element line array, again aligned along the x-axis and in the free field, is assumed and the elevation angle is fixed at broadside. In figure 24, the elevation angle is fixed at 15°, whereas in figure 25, the elevation angle is 30°. In the free field, the optimal directivity of an array of omnidirectional pressure sensors is proportional to the number of array elements, N, for all array steerings. Hence, the constant directivity index of 10 dB for the pressure-sensing array is observed. Notice in figure 23 that the array of uniaxial vector sensors, denoted v_y, provides 3 dB gain over pressure sensors for most azimuthal steering angles. This gain is due to the differences in the cosine and omnidirectional element response patterns. However, at oblique elevation angles, this gain appears to diminish in proportion to the cosine of the elevation angle.

Biaxial and triaxial sensors further improve directivity, particularly for incident angles far from broadside where the gains can be very large. For example, in figure 24 the directivity index of the uniaxial array is 5 dB at 77° azimuth. On the other hand, the triaxial array directivity is 14 dB, providing a directivity gain of 9 dB against isotropic noise. Notice that the maximum gain is achieved when the pressure and all three components of particle velocity are measured and that this optimal gain is constant for all array steerings.
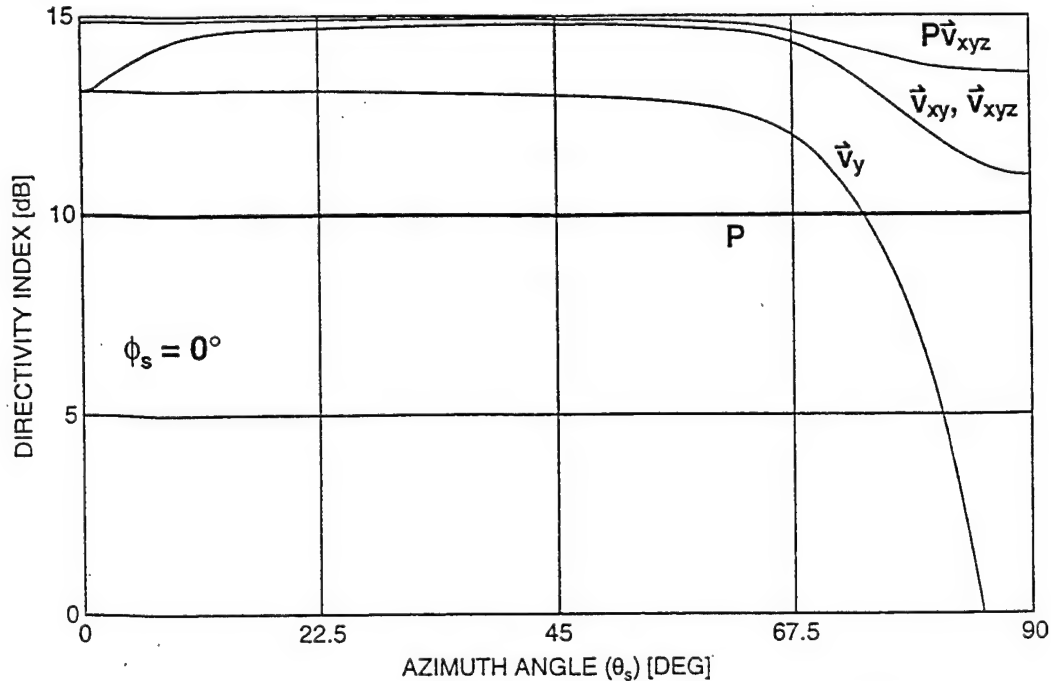
Figure 23. Directivity Versus Azimuthal Angle (θ_S) for a 10-Element Equispaced Line Array at Elevation Angle ($\phi_S = 0°$)

20
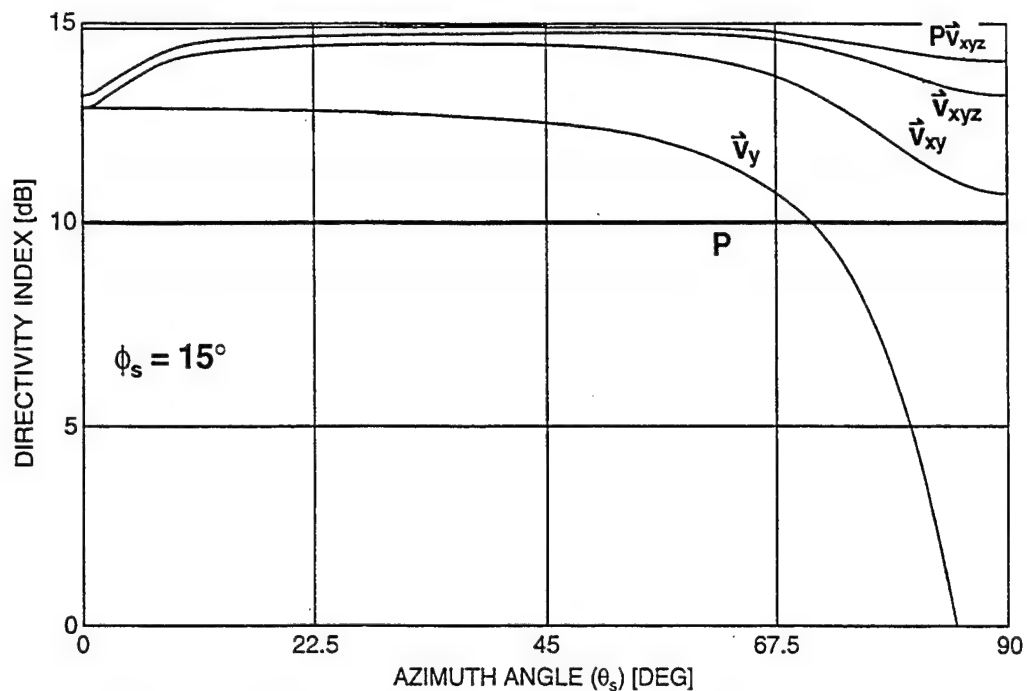
***Figure 24. Directivity Versus Azimuthal Angle (θ_S) for a 10-Element
Equispaced Line Array at Elevation Angle ($\phi_S = 15°$)***
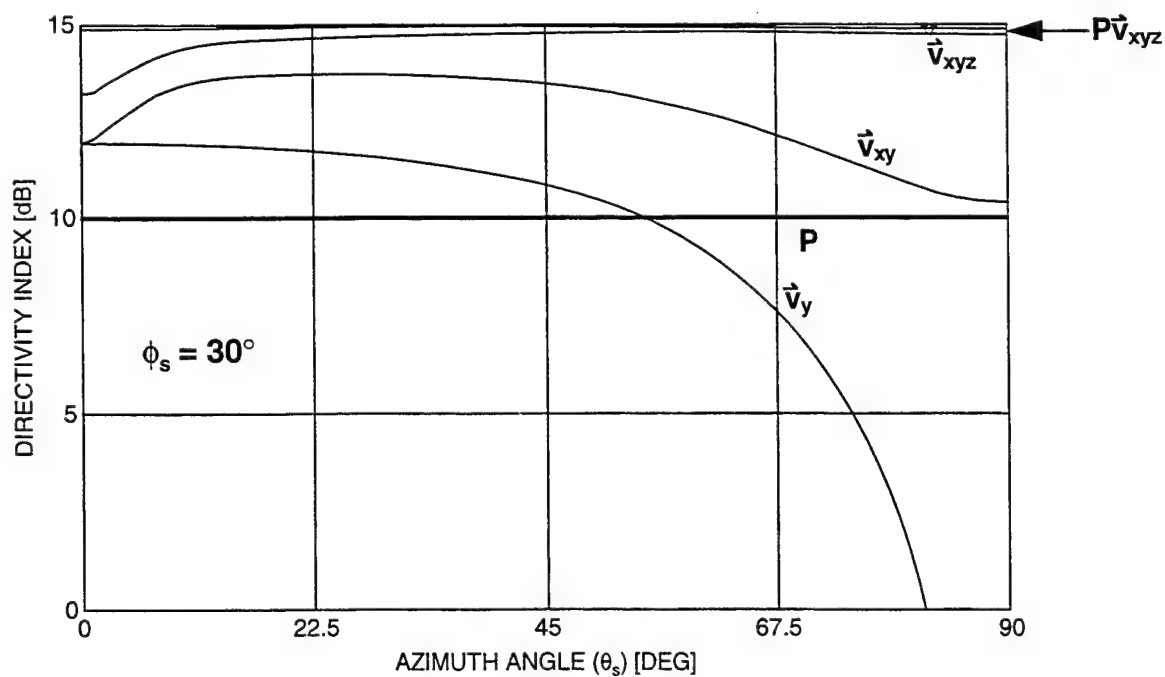
***Figure 25. Directivity Versus Azimuthal Angle (θ_S) for a 10-Element
Equispaced Line Array at Elevation Angle ($\phi_S = 30°$)***

21

THE EFFECT OF ARRAY CURVATURE

Figure 26 depicts a section of a vertical line array, curved about the x-axis, with elements lying in the yz-plane. For this configuration, the component normals $\bar{n}_{y'}$ and $\bar{n}_{z'}$ vary with element position and may be written as

$$\bar{n}_{y'} = \cos(\beta_n)\bar{n}_y + \sin(\beta_n)\bar{n}_z \qquad (35)$$

and

$$\bar{n}_{z'} = -\sin(\beta_n)\bar{n}_y + \cos(\beta_n)\bar{n}_z, \qquad (36)$$

where β_n is the angle formed between the n-th element normal and the y-axis.

Now, the cosine projection angles for the y- and z-velocity components (as in equation (14), taking the dot product of the signal-arrival vector, $\bar{k}$, with the component normals) become

$$\cos(\Theta_{y'}) = \cos(\phi)\cos(\theta)\cos(\beta_n) + \sin(\phi)\ \sin(\beta_n), \qquad (37)$$

and

$$\cos(\Theta_{z'}) = \sin(\phi)\cos(\beta_n) - \cos(\phi)\ \cos(\theta)\sin(\beta_n). \qquad (38)$$
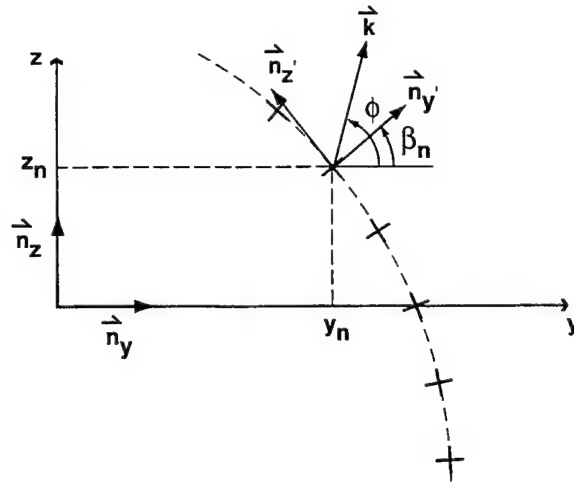
Figure 26. Section of a Curved Vertical Line Array
Comprised of Biaxial Vector Sensors (v_y, v_z) and
Component Normals ($\bar{n}_{y'}$, $\bar{n}_{z'}$)

Using the above result, the signal gain of a curved line array of uniaxial vector sensors, which measures the vector component, v_y, to an array of biaxial sensors, measuring both the v_y- and v_z-components, may be compared. These gains, which are independent of frequency, reveal how curvature and vector element responses combine and affect array performance. The uniaxial and biaxial baffled array sensitivities can be defined, for all steerings, respectively, as

22

$$M_y(\theta_s,\phi_s) = 4\left|\sum_{n=1}^{N} \cos\bigl(\Theta_{y'}(\theta_s,\phi_s)\bigr)w_n(\phi_s)\right|^2 \tag{39}$$

$$M_{yz}(\theta_s,\phi_s) = 4\left|\sum_{n=1}^{N} \left\{\cos^2(\Theta_{y'}(\theta_s,\phi_s)) + \cos^2(\Theta_{z'}(\theta_s,\phi_s))\right\}w_n(\phi_s)\right|^2, \tag{40}$$

where it is recognized that the n-th element shading weight, $w_n(\phi_s)$, may be a function of position and elevation steering angle. The biaxial array sensitivity, M_{yz}, is arbitrarily assumed to have equivalent shading of the v_y and v_z velocity components.

For a given signal power level, the signal gain realized from a curved array of biaxial vector sensors, over that of uniaxial sensors, is defined as

$$SG(\theta_s,\phi_s) = 10 Log_{10}\left\{\frac{M_{yz}(\theta_s,\phi_s)}{M_y(\theta_s,\phi_s)}\right\}. \tag{41}$$

For broadside azimuth steering, the expression for signal gain simplifies to

$$SG(0,\phi_s) = 10 Log_{10}\left\{\frac{\left|\sum_{n=1}^{N} w_n(\phi_s)\right|^2}{\left|\sum_{n=1}^{N} \cos(\phi_s - \beta_n)w_n(\phi_s)\right|^2}\right\}. \tag{42}$$

The signal gain of a fully-populated cylindrically-curved line array, steered to broadside, is given in figure 27. The biaxial sensors improve the conformal array's signal gain at all elevation steerings, providing a minimum gain of approximately 3 dB at ±45° and a maximum gain of nearly 4 dB at both broadside and endfire elevation angles.

23
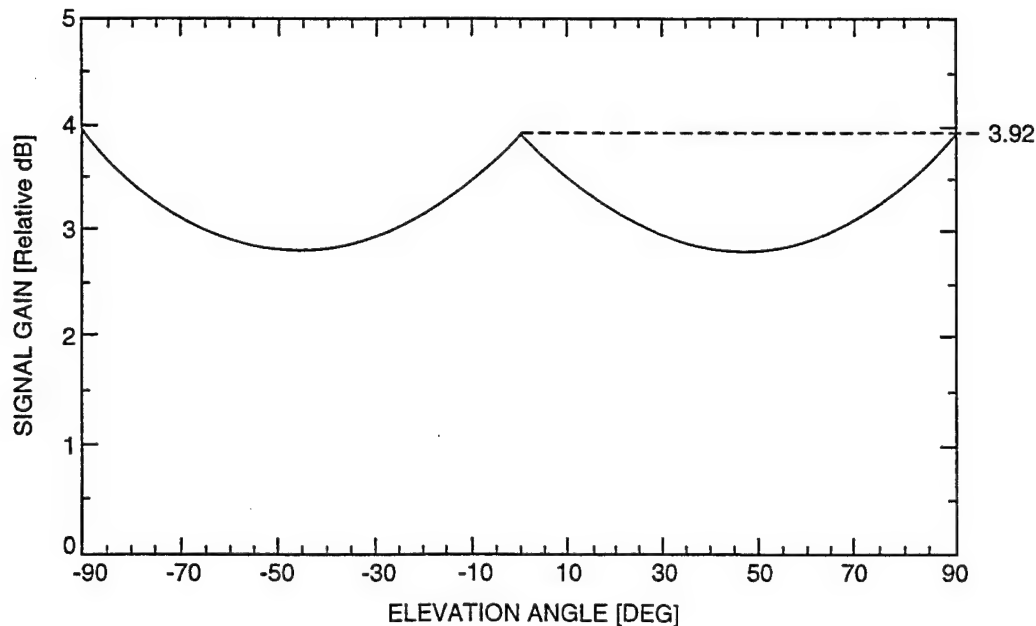
Figure 27. Signal Gain of a Fully-Populated Cylindrically Curved Vertical Line Array of Biaxial Vector Sensors with Uniform Shading Weights

CONCLUSIONS

Presented in this report are formulations for the beam response and directivity of arrays of uniaxial, biaxial, and triaxial vector sensors. To simplify the development, each orthogonal component of a multiaxis vector sensor was assumed to be collocated and the orientation of the components was unvarying from sensor to sensor. However, the amplitude shading coefficients for each vector component of particle velocity was allowed to be arbitrary. The report has investigated the response of the sensors in both the free field and on an ideal baffle.

Of the results presented in this report, the most significant are the increased gains in directivity an array of vector sensors provides, shown in figures 21 through 25, over that of a pressure-sensing array in the free field. Directivity calculations for an ideally-baffled line array is an on-going effort and have not been presented here. Figure 23 indicates that a 10-element line array of triaxial vector sensors, with elements separated by one-half an acoustic wavelength, has a directivity index 5 dB greater than that of an identical line array of pressure sensors for all azimuthal array steerings between 12° to 67°. Hence, to achieve equivalent array gain, the acoustic aperture of the pressure-sensing line array must be almost *four times greater* than that of a vector-sensing array. This implies that vector-sensing arrays, albeit with a larger number of output channels, may be physically smaller than pressure-sensing arrays, without a loss in directivity. With pressure sensors, the only way to increase directivity is to increase array aperture. Therefore, for pressure-sensors, gains in directivity are fundamentally limited by the size of the array. However, for a fixed array aperture and a three-fold increase in channel count, significant directivity gains may be realized with an array of triaxial vector sensors. Increasing the number of processing channels does add complexity and expense to an array design but such design challenges are modest compared to trying to increase array aperture.

24

Another interesting result described here is the ability to form a broad acoustic beam, steered in the direction of an incident signal, using a *single* multiaxis vector sensor. Hence, a vector-sensing line array, oriented say, along the x-axis as shown in figure 1, will provide resolution of both the azimuth and elevation arrival angles. It was noted, however, that the resolution of the elevation angle would be limited to a beamwidth proportional to the cosine of the elevation angle. That is, the beamwidth is $\pm60°$ at the point at which the power relative to the maximum response axis is down by one-half.

Figures 4 and 5 illustrated the angular sensitivity of, respectively, an individual pressure sensor and the y-component of a uniaxial vector sensor. By definition, the uniaxial vector sensor element response is more directional, and it is this directionality which provides the constant 3 dB increase in the array directivity index shown in figure 21. Specifically, the cosine element response has an element directivity that is twice that of an omnidirectional pressure sensor. This gain then, for broadside array steering only, is due simply to the assumed differences in the pressure and uniaxial element responses.

It must be noted that baffled pressure sensors often have an element response pattern approximated well by a cosine raised to a fractional power approaching unity. For these configurations, the directivity index for a linear pressure-sensing array and any type of linear vector-sensing array *steered to broadside*, would be approximately equivalent. A vector-sensing array will provide a constant directivity gain of 3 dB over a pressure-sensing array when it is assumed the pressure sensors are half or omnidirectional. However, additional gains are seen, as shown in figures 23, 24, and 25, for other array steerings. Here, the pressure-sensing directivity remains constant, whereas the multiaxis vector sensor gains vary with array steering and these gains are due to measuring the additional vector components.

A brief investigation of curvature issues indicates that multiaxis vector sensors reduce signal losses due to highly-curved array apertures. An example is given of a fully-populated curved vertical line array comprised of either biaxial vector sensors or uniaxial vector sensors. The biaxial vector sensors improved the signal gain, independent of frequency, over a uniaxial vector sensing array by as much as 4 dB. Similar gains would be seen in a comparison to a pressure-sensing array and, in general, multiaxis vector sensors will improve a conformal array's signal gain for all array steerings.

Finally, it has been shown, particularly in figures 24 and 25, that it is desirable to have an array which measures pressure in addition to the three components of acoustic particle velocity. Optimal processing of arrays which measure all four quantities, pressure and the three components of velocity, is the subject of future research.

APPENDIX A

ANALYTICAL EVALUATION OF DIRECTIVITY
FOR HALF-WAVELENGTH ARRAY SPACING

Array directivity is defined as the ratio of the output signal-to-noise ratio (SNR) of an array to the input SNR at an omnidirectional element in a spherically isotropic noise field. Directivity is a fundamental measure of array performance; the directivity factor, DF, of an array in the free field can be expressed as[6]

$$DF = \frac{4\pi B(\theta_s, \phi_s)}{\int_0^{2\pi} \int_0^{\pi} B(\theta, \phi) \sin(\phi) \, d\phi \, d\theta} ,$$

(A-1)

where $B(\theta, \phi)$ is the array's beam pattern. The directivity index is $10 \log(DF)$. Note that to simplify the following derivations, the elevation angle ϕ will now be measured from the vertical z-axis and the azimuthal angle θ will be measured from the x-axis in the direction of the y-axis. Also, the line array elements are now equispaced along the z-axis at spacing $d = \lambda/2$.

Calculation of the DF typically requires the numerical evaluation of the above double integral. However, for certain array geometries and frequencies (e.g., a frequency at which an acoustic wavelength equals twice the interelement line array spacing, $d_z = \lambda/2$), the integrals may be evaluated exactly. These frequencies correspond to the array's upper aliasing frequency limit and maximum array directivity.

The maximum array response at steering angles (θ_s, ϕ_s) can be obtained from equation (33). In the free field and with elements placed along the z-axis at one-half an acoustic wavelength, the maximum array responses may be written as

$$B_p(\theta_s, \phi_s) = \left| \sum_{n=0}^{N-1} w_n^{(p)} \right|^2 ,$$

(A-2)

$$B_x^{(1)}(\theta_s, \phi_s) = \cos^2(\theta_s) \sin^2(\phi_s) \left| \sum_{n=0}^{N-1} w_n^{(x)} \right|^2 ,$$

(A-3)

$$B_y^{(1)}(\theta_s, \phi_s) = \sin^2(\theta_s) \sin^2(\phi_s) \left| \sum_{n=0}^{N-1} w_n^{(y)} \right|^2 ,$$

(A-4)

$$B_z^{(1)}(\theta_s, \phi_s) = \cos^2(\phi_s) \left| \sum_{n=0}^{N-1} w_n^{(z)} \right|^2, \tag{A-5}$$

and, for triaxial vector sensors,

$$B^{(3)}(\theta_s, \phi_s) = \left| \sum_{n=0}^{N-1} a(\theta_s, \phi_s) w_n^{(x)} + b(\theta_s, \phi_s) w_n^{(y)} + c(\phi_s) w_n^{(z)} \right|^2, \tag{A-6}$$

where $a(\theta_s, \phi_s) = \cos(\theta_s)\sin(\phi_s)$, $b(\theta_s, \phi_s) = \sin(\theta_s)\sin(\phi_s)$, and $c(\phi_s) = \cos(\phi_s)$.

The effort in obtaining expressions for directivity factors then is in analytically evaluating the double integral given in equation (A-1).

DIRECTIVITY FACTORS FOR A SINGLE ELEMENT, N = 1.

It is straightforward to derive the directivity factor of a single omnidirectional pressure sensor. Namely,

$$I = \int_0^{2\pi} \int_0^{\pi} \left| \sum_{n=0}^{N-1} w_n^{(p)} \exp\left\{ in\pi(\cos(\phi) - \cos(\phi_s)) \right\} \right|^2 \sin(\phi)\, d\theta d\phi = 4\pi \left(w_0^{(x)} \right)^2. \tag{A-7}$$

Hence, upon substituting equation (A-7) and (A-2) into equation (A-1),

$$DF_{(p)} = \frac{4\pi (w_0^{(p)})^2}{4\pi (w_0^{(p)})^2} = 1. \tag{A-8}$$

Therefore, the directivity index is zero and the single pressure sensor has no directivity.

A similar calculation for an uniaxial vector sensor that measures the v_x component of particle velocity, as in equation (A-3), gives

$$I = \int_0^{2\pi} \int_0^{\pi} \left(w_0^{(x)} \cos(\theta)\sin(\phi) \right)^2 \sin(\phi)\, d\theta d\phi = \frac{4\pi}{3} \left(w_0^{(x)} \right)^2. \tag{A-9}$$

Upon substitution,

$$DF_{(x)} = 3\cos^2(\theta_s)\sin^2(\phi_s). \tag{A-10}$$

Likewise, for the velocity components v_y and v_z,

$$DF_{(y)} = 3\sin^2(\theta_s)\sin^2(\phi_s), \tag{A-11}$$

and

$$DF_{(z)} = 3\cos^2(\phi_s). \tag{A-12}$$

Equations (A-10), (A-11), and (A-12) indicate that a single velocity sensor may have a maximum directivity factor three times greater than an omnidirectional pressure sensor, or a gain in directivity index of 4.8 dB. (Figures 21 and 22 illustrate this gain.) These results also indicate that directivity factors of vector sensors are also highly dependent on azimuth and elevation angles (θ_s, ϕ_s).

The most general type of single array element would be a triaxial vector sensor augmented with a measurement of pressure, as in equation (33). The maximum response of such an element is given as

$$B_{pv}(\theta_s, \phi_s) = \left(w_0^{(p)} + a(\theta_s, \phi_s)w_0^{(x)} + b(\theta_s, \phi_s)w_0^{(y)} + c(\phi_s)w_0^{(z)} \right)^2, \tag{A-13}$$

and the two-fold integral becomes

$$I = \int_0^{2\pi} \int_0^{\pi} B_{pv}(\theta, \phi)\sin(\phi)\, d\phi d\theta = \frac{4\pi}{3}\left(3(w_0^{(p)})^2 + (w_0^{(x)})^2 + (w_0^{(y)})^2 + (w_0^{(z)})^2 \right). \tag{A-14}$$

Hence, the directivity factor of a single element that measures all 3 components of particle velocity and acoustic pressure is

$$DF_{pv} = \frac{B_{pv}(\theta_s, \phi_s)}{(w_0^{(p)})^2 + \dfrac{(w_0^{(x)})^2}{3} + \dfrac{(w_0^{(y)})^2}{3}\dfrac{(w_0^{(z)})^2}{3}}. \tag{A-15}$$

The goal now becomes determining the weights that maximize the above ratio. Without loss in generality, one may let $w_0^{(p)} = 1$ and solve the following equations simultaneously:

$$\frac{\partial DF_{pv}}{\partial w_0^{(x)}} = \frac{\partial DF_{pv}}{\partial w_0^{(y)}} = \frac{\partial DF_{pv}}{\partial w_0^{(z)}} = 0. \tag{A-16}$$

This leads to two sets of optimal weights, one corresponding to a minimum DF_{pv} and the other, given below, for maximum directivity, i.e.,

$$w_0^{(x)} = 3a(\theta_s, \phi_s), \tag{A-17}$$

$$w_0^{(y)} = 3b(\theta_s, \phi_s),\tag{A-18}$$

$$w_0^{(z)} = 3c(\phi_s).\tag{A-19}$$

Substituting the optimal real weights in equations (A-17), (A-18), and (A-19) into equation (A-15) yields

$$DF_{pv} = 1 + 3\left(a(\theta_s, \phi_s)^2 + b(\theta_s, \phi_s)^2 + c(\phi_s)^2\right) = 4,\tag{A-20}$$

since $a(\theta_s, \phi_s)^2 + b(\theta_s, \phi_s)^2 + c(\phi_s)^2 = 1$ always.

Therefore, the maximum directivity for a single sensor that measures all velocities as well as acoustic pressure is DI = 10 log(4) = 6 dB, and this holds for any steering.

DIRECTIVITY FACTORS FOR AN N-ELEMENT LINE ARRAY

The integral given by equation (A-7) for pressure sensors may be integrated directly over azimuth angle θ, and assuming real-valued weights

$$I = 2\pi \sum_{n=0}^{N-1} \sum_{m=0}^{N-1} w_n^{(p)} w_m^{(p)} \int_0^\pi \exp\left[i(n-m)(\cos(\phi) - \cos(\phi_s))\pi\right] \sin(\phi)\, d\phi.\tag{A-21}$$

Letting $u = \cos(\phi)$ and integrating over u, results in an exact expression for the DF of a line array of pressure sensors, i.e.,

$$DF_p = \frac{\left(\sum_{n=0}^{N-1} w_n^{(p)}\right)^2}{\sum_{n=0}^{N-1} (w_n^{(p)})^2}.\tag{A-22}$$

This ratio is a maximum for uniform weights and results in an optimal directivity of DI = 10 log(N).

Similar analytical expressions for the DF of vector-sensing arrays are difficult to obtain and require one to approximate the DF by assuming a large number of array elements N. For example, consider an array of uniaxial vector sensors that measure the v_y component of particle velocity. Then

$$I = \int_0^{2\pi} \int_0^{\pi} \sin^2(\theta) \sin^2(\phi) \left| \sum_{n=0}^{N-1} w_n^{(y)} \exp\left[in\pi(\cos(\phi) - \cos(\phi_s)) \right] \right|^2 \sin(\phi) \, d\phi \, d\theta. \qquad \text{(A-23)}$$

Letting $u = \cos(\phi)$ and integrating over θ yields

$$I = \pi \int_{-1}^{1} (1 - u^2) \left| \sum_{n=0}^{N-1} w_n^{(y)} e^{in\pi(u - u_s)} \right|^2 du. \qquad \text{(A-24)}$$

Although this integral can be evaluated exactly, it is rather tedious and difficult to interpret and approximate. However, for large N and for $u_s = \cos(\phi_s)$ not close to ± 1, one may argue that the exponential term in equation (A-24) essentially samples (as in a delta function) the integrand at $u = u_s$. Therefore,

$$I \cong \pi(1 - u_s^2) \int_{-1}^{1} \sum_{n=0}^{N-1} \sum_{m=0}^{N-1} w_n^{(y)} w_m^{(y)} e^{i(n-m)\pi(u - u_s)}$$

$$\text{(A-25)}$$

$$= 2\pi \sin^2(\phi_s) \sum_{n=0}^{N-1} (w_n^{(y)})^2.$$

The DF then becomes, substituting (A-4) and (A-25) into (A-1),

$$DF_y = \frac{2\sin^2(\phi_s) \left(\sum_{n=0}^{N-1} w_n^{(y)} \right)^2}{\sum_{n=0}^{N-1} (w_n^{(y)})^2}. \qquad \text{(A-26)}$$

This agrees with the numerical calculations presented in figure 21. This shows that, as the number of array elements increase and for $\phi_s = 90°$, the directivity of a uniaxial vector-sensing array approaches a gain that is 3 dB greater than that of a pressure-sensing array. Approximations for DF_x, DF_z, and even DF_{pv} can be obtained in a similar manner and will be reported in a subsequent report.

APPENDIX B

DERIVATION OF MAXIMUM ARRAY GAIN

Consider an N-element array with pressure sensors and triaxial velocity sensors at each element location x_n, y_n, z_n. It is presumed that each velocity sensor is oriented directly along its corresponding axis. If this array is steered in direction θ_s, ϕ_s by phase shifting the individual element outputs $p_n(t)$, $v_{xn}(t)$, $v_{yn}(t)$, and $v_{zn}(t)$, the most general linearly-processed array output waveform is

$$Y(t) = \sum_{n=1}^{N} e_n^*(\theta_s, \phi_s) \left[w_{pn}\, v_{pn}(t) + w_{xn}\, v_{xn}(t) + w_{yn}\, v_{yn}(t) + w_{zn}\, v_{zn}(t) \right], \qquad \text{(B-1)}$$

where
$$v_{pn}(t) \equiv p_n(t)/(\rho c), \quad k = \omega/c,$$

$$e_n(\theta, \phi) \equiv \exp\left[ik(x_n\, \sin\phi\, \cos\theta + y_n\, \sin\phi\, \sin\theta + z_n\, \cos\phi) \right], \qquad \text{(B-2)}$$

and the 4N weights $\{w_{pn}\}$, $\{w_{xn}\}$, $\{w_{yn}\}$, $\{w_{zn}\}$ are real, but otherwise arbitrary.

A plane-wave signal arrival from direction θ_a, ϕ_a results in the array output signal waveform

$$Y(t) = V_1 \exp(i\omega t) \sum_{n=1}^{N} e_n^*(\theta_s, \phi_s)\, e_n(\theta_a, \phi_a) \left[w_{pn} + \right.$$

$$\left. + w_{xn} \sin\phi_a \cos\theta_a + w_{yn} \sin\phi_a \sin\theta_a + w_{zn} \cos\phi_a \right], \qquad \text{(B-3)}$$

where $V_1 \exp(i\omega t)$ is the pressure waveform observed at the origin of coordinates. For notational convenience, define the direction cosines

$$D_x = \sin\phi \cos\theta, \quad D_y = \sin\phi \sin\theta, \quad D_z = \cos\phi, \qquad \text{(B-4)}$$

and the two 4Nx1 real column matrices

$$W = [w_{p1}\ldots \quad w_{pN} \quad w_{x1}\ldots \quad w_{xN} \quad w_{y1}\ldots \quad w_{yN} \quad w_{z1}\ldots \quad w_{zN}]^T,$$

$$\text{(B-5)}$$

$$D(\theta, \phi) = [\,1\ldots \quad 1 \quad D_x \ldots \quad D_x \quad D_y \ldots \quad D_y \quad D_z \ldots \quad D_z]^T.$$

Then, when the plane-wave signal arrival angle coincides with the steering angle, namely, $\theta_a = \theta_s$, $\phi_a = \phi_s$, the array signal output waveform is expressible as

$$Y_1(t) = V_1 \exp(i\omega t) W^T D(\theta_s, \phi_s). \tag{B-6}$$

The array signal output power is then

$$P_{so} = |Y_1(t)|^2 = |V_1|^2 \left[W^T D(\theta_s, \phi_s) \right]^2. \tag{B-7}$$

At the same time, the array output noise waveform can be expressed as

$$Y_o(t) = W^T V_o(t), \tag{B-8}$$

the 4Nx1 column matrix

$$V_o(t) = \begin{bmatrix} V_p(t) \\ V_x(t) \\ V_y(t) \\ V_z(t) \end{bmatrix}, \tag{B-9}$$

and the four Nx1 column matrices

$$V_p(t) \equiv \left[e_1^*(\theta_s, \phi_s) v_{p1}(t) \dots e_N^*(\theta_s, \phi_s) v_{pN}(t) \right]^T,$$

$$V_x(t) \equiv \left[e_1^*(\theta_s, \phi_s) v_{x1}(t) \dots e_N^*(\theta_s, \phi_s) v_{xN}(t) \right]^T,$$

$$\tag{B-10}$$

$$V_y(t) \equiv \left[e_1^*(\theta_s, \phi_s) v_{y1}(t) \dots e_N^*(\theta_s, \phi_s) v_{yN}(t) \right]^T,$$

$$V_z(t) \equiv \left[e_1^*(\theta_s, \phi_s) v_{z1}(t) \dots e_N^*(\theta_s, \phi_s) v_{zN}(t) \right]^T.$$

This leads to the array output noise power in the form

$$P_{no} = \overline{|Y_o(t)|^2} = W^T \overline{V_o(t) V_o^H(t)} W = W^T R W, \tag{B-11}$$

where R is a Hermitian 4Nx4N covariance matrix of the totality of 4N received noise waveforms. Because all the weights in (B-1) and (B-5) are real, (B-11) can be written as

$$P_{no} = W^T R_r W;$$ (B-12)

that is, the imaginary part of R is not active in Hermitian form (B-11).

We define the array gain as the quotient of the output signal-to-noise ratio to the input signal-to-noise ratio. There follows

$$AG = \frac{[W^T D(\theta_s, \phi_s)]^2}{W^T R_r W},$$ (B-13)

where we have normalized the input noise pressure power at unity.

The 4N optimum weights that maximize this array gain are

$$W_o = \alpha R_r^{-1} D(\theta_s, \phi_s),$$ (B-14)

while the corresponding optimum array gain is

$$AG_o = \max AG = D^T(\theta_s, \phi_s) R_r^{-1} D(\theta_s, \phi_s).$$ (B-15)

This relation was used in the main body of the report to obtain the numerical values in figures 21 through 25. The elements of the real 4Nx4N matrix R_r are given in Appendix C.

APPENDIX C

SENSOR CORRELATIONS IN AN ISOTROPIC NOISE FIELD

In this appendix, ϕ is the polar angle measured down from the vertical z-axis, while θ is the azimuthal angle measured from the x-axis in the direction of the y-axis.

FUNDAMENTAL DOUBLE INTEGRAL

$$\int_0^\pi d\phi \, \sin\phi \int_0^{2\pi} d\theta \, \exp(ia \, \sin\phi \, \cos\theta + ib \, \sin\phi \, \sin\theta + ic \, \cos\phi)$$

$$= 2\pi \int_0^\pi d\phi \, \sin\phi \, \exp(ic \, \cos\phi) \, J_0\left((a^2 + b^2)^{1/2} \sin\phi\right)$$

$$= 2\pi \int_0^\pi d\phi \, \sin\phi \, \cos(c \, \cos\phi) \, J_0\left((a^2 + b^2)^{1/2} \sin\phi\right)$$

$$= 4\pi \int_0^{\pi/2} d\phi \, \sin\phi \, \cos(c \, \cos\phi) \, J_0\left((a^2 + b^2)^{1/2} \sin\phi\right)$$

$$= 4\pi \frac{\sin Q}{Q}, \qquad Q = (a^2 + b^2 + c^2)^{1/2},$$

where [7; 6.688 2] is used in the last line. Also used is the fact that $\sin(c \, \cos\phi)$ is odd in ϕ about $\phi = \pi/2$, whereas all the other functions are even in ϕ about $\phi = \pi/2$. This result applies for complex a, b, c as well.

It is now possible to evaluate, in closed form, extensions of the double integral above to include additional factors of the form

$$(\sin\phi \, \cos\theta)^m (\sin\phi \, \sin\theta)^n (\cos\phi)^k,$$

where m, n, k are integers, by taking partial derivatives with respect to a and/or b and/or c. To that aim, let

$$F = \frac{\sin Q}{Q} = j_0(Q).$$

Then,

$$F_a \equiv \frac{\partial}{\partial a} F = \frac{dF}{dQ} \frac{\partial Q}{\partial a} = \left[\frac{\cos Q}{Q^2} - \frac{\sin Q}{Q^3} \right] a = -a \, j_1(Q)/Q \, ;$$

here the term $\partial Q/\partial a = a/Q$ is used. The bracketed term is -1/3 at $Q = 0$. Also,

$$F_{ab} \equiv \frac{\partial}{\partial b} F_a = \left[\frac{(3-Q^2)\sin Q - 3Q \cos Q}{Q^5} \right] ab = ab \, j_2(Q)/Q^2 \, ,$$

where the bracketed term is 1/15 at $Q = 0$. Finally,

$$F_{aa} \equiv \frac{\partial}{\partial a} F_a = \left[\frac{\cos Q}{Q^2} - \frac{\sin Q}{Q^3} \right] + \left[\frac{(3-Q^2)\sin Q - 3Q \cos Q}{Q^5} \right] a^2$$

$$= -j_1(Q)/Q + a^2 \, j_2(Q)/Q^2 \, .$$

All other partial derivatives of first and second order, with respect to a and/or b and/or c, follow from these results by use of symmetry; that is, $Q = (a^2 + b^2 + c^2)^{1/2}$. The following is an example of their immediate application:

$$-\frac{1}{4\pi} \int_0^\pi d\phi \, \sin \phi \int_0^{2\pi} d\theta \, (\sin \phi \, \cos \theta) \quad (\sin \phi \, \sin \theta)$$

$$\times \exp(ia \sin \phi \, \cos \theta + ib \sin \phi \, \sin \theta + ic \cos \phi) = F_{ab} \, .$$

SPHERICALLY-ISOTROPIC NOISE PRESSURE FIELD

Let the incident pressure at the origin of coordinates, due to incremental solid angle $d\theta \, d\phi$ about arrival angle θ, ϕ, be

$$dp(t,0,0,0) = \exp(i\omega t) \, P(\theta, \phi) \, d\theta \, d\phi \, ,$$

where noise source distribution $P(\theta, \phi)$ is zero mean and satisfies

$$\overline{P(\theta, \phi) \, P*(\theta', \phi')} = I \sin\phi \, \delta(\theta - \theta') \, \delta(\phi - \phi') \, .$$

This corresponds to an isotropic noise field of uncorrelated arrivals where I is a measure of the intensity (and could be a function of ω), while the $\sin\phi$ factor is due to the incremental surface area in spherical coordinates.

The incremental pressure at general point $P_1 = (x_1, y_1, z_1)$ is then

$$dp(t, x_1, y_1, z_1) = dp(t - \tau_1(\theta, \phi), 0, 0, 0),$$

where time delay

$$\tau_1(\theta, \phi) = -\frac{1}{c}\left(x_1 \sin\phi \cos\theta + y_1 \sin\phi \sin\theta + z_1 \cos\phi\right).$$

The total (noise) pressure at P_1 is, therefore, with $k = \omega/c$,

$$\mathbf{p}(t, x_1, y_1, z_1) = \exp(i\omega t) \int_0^\pi d\phi \int_0^{2\pi} d\theta\, \mathbf{P}(\theta, \phi)$$

$$\times \exp\left[ik\left(x_1 \sin\phi \cos\theta + y_1 \sin\phi \sin\theta + z_1 \cos\phi\right)\right].$$

The correlation of pressures at separated times and distances is

$$\overline{\mathbf{p}(t_1, x_1, y_1, z_1)\mathbf{p}^*(t_2, x_2, y_2, z_2)} = \exp[i\omega(t_1 - t_2)] \int_0^\pi d\phi \int_0^{2\pi} d\theta$$

$$\times \int_0^\pi d\phi' \int_0^{2\pi} d\theta'\, \overline{\mathbf{P}(\theta, \phi)\mathbf{P}^*(\theta', \phi')} \exp\left[ik\left(x_1 \sin\phi \cos\theta + y_1 \sin\phi \sin\theta\right.\right.$$

$$\left.\left. + z_1 \cos\phi - x_2 \sin\phi' \cos\theta' - y_2 \sin\phi' \sin\theta' - z_2 \cos\phi'\right)\right]$$

$$= I \exp[i\omega(t_1 - t_2)] \int_0^\pi d\phi \sin\phi \int_0^{2\pi} d\theta \exp\left[ik(\{x_1 - x_2\}\sin\phi \cos\theta\right.$$

$$\left. +\{y_1 - y_2\}\sin\phi \sin\theta + \{z_1 - z_2\}\cos\phi)\right]$$

$$= 4\pi\, I \exp[i\omega(t_1 - t_2)]\, \frac{\sin(kd)}{kd},$$

where

$$d = \left[(x_1 - x_2)^2 + (y_1 - y_2)^2 + (z_1 - z_2)^2\right]^{1/2}.$$

This correlation has the familiar $\sin(kd)/(kd)$ spatial behavior, where d is the absolute distance between the two points of interest; this statement is in coordinate-free form, since distance d is independent of the particular geometry adopted.

ISOTROPIC NOISE VELOCITY FIELD

Let $\vec{u}(\theta,\phi)$ be the unit vector pointing in direction θ,ϕ:

$$\vec{u}(\theta,\phi) = \sin\phi \, \cos\theta \, \vec{i} + \sin\phi \, \sin\theta \, \vec{j} + \cos\phi \, \vec{k}.$$

Let the incident velocity field at the origin of coordinates, due to incremental solid angle $d\theta \, d\phi$ about arrival angle θ,ϕ, be

$$d\vec{v}(t,0,0,0) = \exp(i\omega t) \, S(\theta,\phi) \, d\theta \, d\phi \, \vec{u}(\theta,\phi),$$

where noise source distribution $S(\theta,\phi)$ is zero mean and satisfies

$$\overline{S(\theta,\phi) \, S^*(\theta',\phi')} = I \sin\phi \, \delta(\theta-\theta') \, \delta(\phi-\phi').$$

This corresponds to an isotropic noise field of uncorrelated arrivals where I is a measure of the intensity (and could be a function of ω), while the $\sin\phi$ factor is due to the incremental surface area in spherical coordinates.

The incremental velocity at general point $P_1 = (x_1, y_1, z_1)$ is then

$$d\vec{v}(t, x_1, y_1, z_1) = d\vec{v}(t - \tau_1(\theta,\phi), 0, 0, 0),$$

where the time delay is

$$\tau_1(\theta,\phi) = -\frac{1}{c}\left(x_1 \sin\phi \, \cos\theta + y_1 \sin\phi \, \sin\theta + z_1 \cos\phi\right).$$

The total (noise) velocity at P_1 is, therefore, with $k = \omega/c$,

$$\vec{v}(t, x_1, y_1, z_1) = \exp(i\omega t) \int_0^\pi d\phi \int_0^{2\pi} d\theta \, S(\theta,\phi)$$

$$\times \exp\left[ik(x_1 \sin\phi \, \cos\theta + y_1 \sin\phi \, \sin\theta + z_1 \cos\phi)\right] \vec{u}(\theta,\phi).$$

If $\exp[\ ]$ denotes the spatial exponential term above, and the velocity vector is expanded as $\vec{v} = v_x \, \vec{i} + v_y \, \vec{j} + v_z \, \vec{k}$, then the velocity components at P_1 are

$$\mathbf{v}_x(t,x_1,y_1,z_1) = \exp(i\omega t) \int_0^{\pi} d\phi \int_0^{2\pi} d\theta \, \mathbf{S}(\theta,\phi) \exp[\;] \sin\phi \, \cos\theta \, ,$$

$$\mathbf{v}_y(t,x_1,y_1,z_1) = \exp(i\omega t) \int_0^{\pi} d\phi \int_0^{2\pi} d\theta \, \mathbf{S}(\theta,\phi) \exp[\;] \sin\phi \, \sin\theta \, ,$$

$$\mathbf{v}_z(t,x_1,y_1,z_1) = \exp(i\omega t) \int_0^{\pi} d\phi \int_0^{2\pi} d\theta \, \mathbf{S}(\theta,\phi) \exp[\;] \cos\phi \, .$$

We are interested in all six possible correlations at general separated times and distances, namely

$$\overline{\mathbf{v}_x(t_1,x_1,y_1,z_1)\,\mathbf{v}_y^*(t_2,x_2,y_2,z_2)}\,,$$

$$\overline{\mathbf{v}_x\mathbf{v}_z^*}\,,\quad \overline{\mathbf{v}_y\mathbf{v}_z^*}\,,\quad \overline{\mathbf{v}_x\mathbf{v}_x^*}\,,\quad \overline{\mathbf{v}_y\mathbf{v}_y^*}\,,\quad \overline{\mathbf{v}_z\mathbf{v}_z^*}\,,$$

where an abbreviated notation has been employed in the latter line.

The xy-correlation is

$$\overline{\mathbf{v}_x(t_1,x_1,y_1,z_1)\mathbf{v}_y^*(t_2,x_2,y_2,z_2)} = \exp[i\omega(t_1-t_2)]\int_0^{\pi} d\phi \int_0^{2\pi} d\theta \, I \sin\phi$$

$$\times (\sin\phi\cos\theta)\,(\sin\phi\sin\theta)\exp\big[ik(\{x_1-x_2\}\sin\phi\cos\theta$$

$$+\,\{y_1-y_2\}\sin\phi\sin\theta + \{z_1-z_2\}\cos\phi)\big] = -4\pi\,F_{ab}\,I\exp[i\omega(t_1-t_2)]$$

$$= 4\pi\,I\exp[i\omega(t_1-t_2)]\frac{(Q^2-3)\sin Q + 3Q\cos Q}{Q^5}\,k^2(x_1-x_2)(y_1-y_2)$$

$$= -4\pi\,I\exp[i\omega(t_1-t_2)]\,\frac{j_2(Q)}{Q^2}\,k^2(x_1-x_2)(y_1-y_2)\,,$$

where

$$Q = kd = k\left[(x_1-x_2)^2 + (y_1-y_2)^2 + (z_1-z_2)^2\right]^{1/2}.$$

Here, the delta function properties of the correlation function of random field $\mathbf{S}(\theta,\phi)$ and the double integral results derived above are used. The ratio $j_2(Q)/Q^2$ is 1/15 at $Q=0$.

It should be observed that the xy correlation involves the factor $(x_1 - x_2)(y_1 - y_2)$, in addition to the symmetric function Q of all the spatial differences. Therefore, by symmetry, the xz correlation is identical to that above, except that factor $(x_1 - x_2)(y_1 - y_2)$ is replaced by $(x_1 - x_2)(z_1 - z_2)$. A similar replacement of this factor holds for the yz correlation.

The other type of (auto) correlation of interest can be represented by the quantity

$$\overline{\mathbf{v}_x(t_1, x_1, y_1, z_1)\mathbf{v}_x^*(t_2, x_2, y_2, z_2)} = \exp[i\omega(t_1 - t_2)]\int_0^\pi d\phi \int_0^{2\pi} d\theta \, I \sin\phi$$

$$\times (\sin\phi \cos\theta)^2 \exp\left[ik(\{x_1 - x_2\}\sin\phi\cos\theta + \{y_1 - y_2\}\sin\phi\sin\theta + \{z_1 - z_2\}\cos\phi)\right]$$

$$= -4\pi \, F_{aa} \, I \exp[i\omega(t_1 - t_2)]$$

$$= E\left(\frac{\sin Q}{Q^3} - \frac{\cos Q}{Q^2} + \frac{(Q^2 - 3)\sin Q + 3Q\cos Q}{Q^5}k^2(x_1 - x_2)^2\right)$$

$$= E\left(\frac{j_1(Q)}{Q} - \frac{j_2(Q)}{Q^2}k^2(x_1 - x_2)^2\right),$$

where

$$E \equiv 4\pi \, I \exp\left[i\omega\left(t_1 - t_2\right)\right].$$

Again, by use of the symmetric behavior of Q, the yy correlation follows immediately upon replacement of the $(x_1 - x_2)^2$ factor by $(y_1 - y_2)^2$. A similar procedure holds for zz correlation.

When points P_1 and P_2 coincide, $Q = 0$ and all three (auto) correlations reduce to $E/3$; here, $j_1(Q)/Q = 1/3$ is used at $Q = 0$. This observation is consistent with the fact that the field is isotropic and no coordinate direction is preferred, in so far as one point in space is concerned.

ONE POINT IN SPACE

Now, some of the general results above will be specialized. For one point in space, set $x_2 = x_1, y_2 = y_1, z_2 = z_1$, getting $Q = 0$ and

$$\overline{\mathbf{v}_x(t_1,x_1,y_1,z_1)\mathbf{v}_y^*(t_2,x_1,y_1,z_1)} = 0$$

$$\overline{\mathbf{v}_x(t_1,x_1,y_1,z_1)\mathbf{v}_z^*(t_2,x_1,y_1,z_1)} = 0 \left.\right\} \quad \text{for all } t_1, t_2, x_1, y_1, z_1.$$

$$\overline{\mathbf{v}_y(t_1,x_1,y_1,z_1)\mathbf{v}_z^*(t_2,x_1,y_1,z_1)} = 0$$

Also, there follows

$$\overline{\mathbf{v}_w(t_1,x_1,y_1,z_1)\mathbf{v}_w^*(t_2,x_1,y_1,z_1)} = \frac{E}{3} = \frac{4\pi}{3} I \exp[i\omega(t_1 - t_2)],$$

where subscript $w = x$ or y or z.

Since the coordinate axes are arbitrary, these properties can be summarized in a coordinate-free form: for any orthogonal cartesian coordinate system, the three velocity components at one spatial point are uncorrelated with each other for all time delays. Also, each velocity component has identical time (auto) correlations.

TWO DIFFERENT POINTS IN SPACE

Consider two points P_1 and P_2 in space. If an arbitrary cartesian coordinate system is erected, the two locations $P_1 = (x_1, y_1, z_1)$ and $P_2 = (x_2, y_2, z_2)$ will not have any special properties; that is, $x_2 \neq x_1$, $y_2 \neq y_1$, $z_2 \neq z_1$. Then, none of the correlations above (auto or cross) will be zero. Physically, this says that, generally, all of the three orthogonal velocity components at P_1 are correlated with all of the three orthogonal velocity components at P_2.

However, there is one special coordinate choice which does have uncorrelated velocity components. Since the noise field is isotropic, there is no loss of generality in taking the z-axis to be parallel to the line joining points P_1 and P_2; this still leaves rotational freedom for the locations of the perpendicular x- and y-axes. Thus, $\mathbf{v}_z(t_1, x_1, y_1, z_1)$ is called the in-line velocity component at point P_1 at time t_1, i.e., the velocity at P_1 along the line joining points P_1 and P_2. Then, $\mathbf{v}_x(t_1, x_1, y_1, z_1)$ and $\mathbf{v}_y(t_1, x_1, y_1, z_1)$ are called the two in-plane velocity components at P_1 at time t_1, namely, the orthogonal velocities in the plane perpendicular to the z-axis at location $z = z_1$. Recall that the location of the x- and y-axes is arbitrary.

Now,

$$x_2 = x_1, \quad y_2 = y_1, \quad Q = k|z_1 - z_2| = kd,$$

where d is the distance between point P_1 and P_2. There follows

$$\overline{\mathbf{v}_x(t_1,x_1,y_1,z_1)\mathbf{v}_y^*(t_2,x_1,y_1,z_2)} = 0$$

$$\overline{\mathbf{v}_x(t_1,x_1,y_1,z_1)\mathbf{v}_z^*(t_2,x_1,y_1,z_2)} = 0 \Big\} \quad \textit{for all } t_1,t_2,x_1,y_1,z_1,z_2 .$$

$$\overline{\mathbf{v}_y(t_1,x_1,y_1,z_1)\mathbf{v}_z^*(t_2,x_1,y_1,z_2)} = 0$$

Stated in a coordinate-free form, the in-line velocity component at P_2 is uncorrelated with all in-plane velocity components at P_1 for all time delays and distance separations d. Also, any in-plane velocity component at P_2 is uncorrelated with its orthogonal in-plane velocity component at P_1 for all time delays and distance separations d.

In addition, for all t_1,t_2,x_1,y_1,z_1,z_2, the correlations are

$$\overline{\mathbf{v}_x(t_1,x_1,y_1,z_1)\mathbf{v}_x^*(t_2,x_1,y_1,z_2)} = E\left(\frac{\sin Q}{Q^3} - \frac{\cos Q}{Q^2}\right) = E\frac{j_1(Q)}{Q} ,$$

$$\overline{\mathbf{v}_y(t_1,x_1,y_1,z_1)\mathbf{v}_y^*(t_2,x_1,y_1,z_2)} = E\left(\frac{\sin Q}{Q^3} - \frac{\cos Q}{Q^2}\right) = E\frac{j_1(Q)}{Q} ,$$

$$\overline{\mathbf{v}_z(t_1,x_1,y_1,z_1)\mathbf{v}_z^*(t_2,x_1,y_1,z_2)} = E\left(\frac{Q^2 - 2)\sin Q + 2Q\cos Q}{Q^3}\right)$$

$$= E\left(\frac{j_1(Q)}{Q} - j_2(Q)\right) = E\left(j_0(Q) - 2\frac{j_1(Q)}{Q}\right) ,$$

where $Q = kd$ and $E = 4\pi I \exp[i\omega(t_1-t_2)]$. That is, the orthogonal in-plane velocity components have identical spatial correlations, whereas that for the in-line velocity component is different.

All three (auto) correlations reduce to $E/3 = 4\pi/3\ I \exp[i\omega(t_1-t_2)]$ at $z_2 = z_1$, making $P_2 = P_1$, a common point. On the other hand, for large physical separations d, the in-plane correlations behave as $-E \cos Q/Q^2$, whereas the in-line correlation decays slower, namely, as $E \sin Q/Q$. This latter form is identical to the pressure correlation in an isotropic field.

REFERENCES

1. G. L. D'Spain et al., "Initial Analysis of the Data from the Vertical DIFAR Array," *Proceedings of Mastering the Oceans Through Technology, (OCEANS 92)*, Newport, Rhode Island, October 26-29, 1992.

2. A. Nehorai and E. Paldi, "Acoustic Vector-Sensor Array Processing," *IEEE Trans. on Signal Processing*, vol. 42(9), September 1994.

3. M. Hawkes and A. Nehorai, "Surface-Mounted Acoustic Vector-Sensor Array Processing," *IEEE International Conference on Acoustics, Speech and Signal Processing (ICASSP96)*, May 1996.

4. R. Kneipfer, "Array Processing for Detection of Narrowband, Planewave Velocity Fields," Unpublished Memorandum, Naval Undersea Warfare Center Detachment, New London, CT, March 1996.

5. R. F. Keltie, "Response of Elastically-Coasted Plates to Incident Acoustic Plane Waves," IPA Activity Report, North Carolina State University, Raleigh, NC, 1 November 1996.

6. A. H. Nuttall and B. A. Cray, "Efficient Calculation of Directivity Indices for Certain Three-Dimensional Arrays," NUWC-NPT Technical Report 11,129, Naval Undersea Warfare Center Detachment, New London, CT, 26 July 1996.

7. I. S. Gradshteyn and I. M. Ryzhik, *Table of Integrals, Series, and Products*, Academic Press, Inc., New York, NY, 1980.

INITIAL DISTRIBUTION LIST

Addressee	No. of Copies
Naval Sea Systems Command (PEO-USW-ASTO, CDR J. Polcari, M. Traweek)	2
Office of Naval Research (334, V. Simmons; 331SS, R. Varley, K. Dial; 321 US, J. Tague)	4
Bolt, Beranek and Newman (N. Martin, R. Brown)	2
Litton Guidance and Control Systems (S. Martin)	1
North Carolina State University (R. Keltie)	1
University of Illinois-Chicago (A. Nehorai)	1
Scripps Institution of Oceanography (G. D'Spain)	1
Defense Technical Information Center	2